PREPARATION AND CHARACTERIZATION OF SILVER SERS NANOTAGS

A THESIS SUBMITTED TO
THE GRADUATE SCHOOL OF NATURAL AND APPLIED SCIENCES
OF
MIDDLE EAST TECHNICAL UNIVERSITY

BY

SEDA KİBAR

IN PARTIAL FULFILLMENT OF THE REQUIREMENTS
FOR
THE DEGREE OF MASTER OF SCIENCE
IN
CHEMISTRY

DECEMBER, 2010

Approval of the Thesis;

PREPARATION AND CHARACTERIZATION OF SILVER SERS NANOTAGS

submitted by **SEDA KİBAR** in a partial fulfillment of the requirements for the degree of **Master of Science in Chemistry Department, Middle East Technical University** by

Prof. Dr. Canan Özgen
Dean, Graduate School of **Natural and Applied Sciences** _____

Prof. Dr. İlker Özkan
Head of Department, **Chemistry** _____

Prof Dr. Mürvet Volkan
Supervisor, **Chemistry Department, METU** _____

Examining Committee Members:

Prof Dr. O. Yavuz Ataman
Chemistry Department, METU _____

Prof Dr. Mürvet Volkan
Chemistry Department, METU _____

Prof Dr. Macit Özenbaş
Metallurgical and Materials Engineering Department, METU _____

Prof Dr. Semra Kocabıyık
Biology Department, METU _____

Assoc. Prof. Dr. Nursen Çoruh
Chemistry Department, METU _____

Date: December 17, 2010

I hereby declare that all information in this document has been obtained and presented in accordance with academic rules and ethical conduct. I also declare that, as required by these rules and conduct, I have fully cited and referenced all material and results that are not original to this work.

Name, Last Name: Seda Kibar

Signature:

ABSTRACT

PREPARATION AND CHARACTERIZATION OF SILVER SERS NANOTAGS

Kibar, Seda

M.S., Department of Chemistry

Supervisor: Prof. Dr. Mürvet Volkan

December 2010, 88 pages

Tags are materials used for labeling substances and so make possible the qualitative and quantitative analysis both in macroscopic and microscopic world. Nowadays, surface enhanced Raman spectroscopy became the favored one among the optical based-tag detection systems. Progress in surface enhanced Raman detection and imaging technologies depends on the availability of Raman labels with strong light scattering characteristics.

In this study various SERS nanotags were prepared. An ideal SERS nanotag consists of three parts, core nanoparticle for enhancement, Raman active molecule for signature and a shell for protection and further functionalization.

As a core material, silver nanoparticles were prepared using the chemical reduction method with sodium citrate as reductant. SERS enhancement provided by Ag particles

prepared was examined. For colloidal stabilization and further surface modifications, silica with a controlled thickness was deposited on Ag nanoparticles.

Three single-dye doped nanotags, Ag-BCB@SiO_2 Ag-CFV@SiO_2 and Ag-CV@SiO_2 were prepared using positively charged dyes, brilliant cresyl blue (BCB), cresyl fast violet (CFV) and cresyl violet (CV). The effects of silica thickness and dye concentration in the reaction medium were examined. Stability of prepared nanotags and repeatability of the method were investigated.

Multi-dye doped nanotags were prepared using BCB and CFV solutions mixed at various concentration ratios. Resulting Raman spectra Ag-BCB-CFV@SiO_2 nanotags successfully exhibited characteristic peaks of each dye with a good resolution. In addition, the molar ratio between dyes BCB and CFV was reflected on the related spectra. A linear correlation was observed between the molar ratio of the dyes and their Raman intensity ratio.

Keywords: Nanoparticle, nanotag, surface enhanced Raman spectroscopy, single-dye doped nanotag, multi-dye doped nanotag, multiplex analysis.

ÖZ

YÜZEYDE GÜÇLENDİRİLMİŞ RAMAN SPEKTROSKOPİ İÇİN GÜMÜŞ NANO-ETİKETLERİN HAZIRLANMASI VE KARAKTERİZASYONU

Kibar, Seda

Yüksek Lisans, Kimya Bölümü

Tez Yöneticisi: Prof. Dr. Mürvet Volkan

Aralık 2010, 88 sayfa

Etiketler, bağlandıklara moleküllere imzalarını taşıyarak makroskopik ve mikroskopik dünyasında nitel ve nicel olarak tayini mümkün kılan maddelerdir. Son günlerde, Yüzeyde Güçlendirilmiş Raman Spektroskopisi, optik dayanıklı-etiket sistemleri içerisinde favori haline gelmiştir. Yüzeyde Güçlendirilmiş Raman tayinleri ve görüntüleme teknolojilerindeki ilerleme, güçlü ışık saçılım özelliği taşıyan Raman etiketlerin elde edilebirliğine bağlıdır.

Bu çalışmada, çeşitli YGRS nano etiketler hazırlanmıştır. İdeal bir YGRS nano etiketi, güçlendirme için çekirdek nanoparçacık, imza için Raman aktif molekül ve koruma ve ileri yüzey modifikasyonlar için tabaka olmak üzere üç parçadan oluşmaktadır.

Çekirdek malzeme olarak, gümüş nanoparçacıklar, sodyum sitratın indirgeyici olarak kullanıldığı kimyasal indirgeme metodu takip edilerek hazırlanmıştır. Hazırlanan Ag parçacıkların sağladığı güçlendirme araştırılmıştır. Ag parçacıkları, kolloidsel kararlılık ve ileri yüzey modifikasyonları için kontrol edilebilir kalınlıkta silika ile kaplanmıştır.

Poiztif yüklü boyalar olan brilliant cresyl blue (BCB), cresyl fast violet (CFV) ve cresyl violet (CV) kullanılarak Ag-BCB@SiO_2 Ag-CFV@SiO_2 ve Ag-CV@SiO_2 olmak üzere üç farklı tek boya gömülü nano etiketler hazırlanmıştır. Silika kalınlığı ve reaksiyon ortamındaki boya derişiminin silica kalınlığına olan etkisi incelenmiştir. Hazırlanan nano etiketlerin kararlılığı ve kullanılan metodun tekraranabilirliği çalışılmıştır.

Çoklu boya gömülü nano etiketler, BCB ve CFV çözeltileri çeşitli oranlarda karıştırılarak hazırlanmıştır. Elde edilen Ag-BCB-CFV@SiO_2 nano etiketlerin Raman spektrumları, her iki boyanın tipik piklerini iyi bir ayrımla başarıyla sergilemiştir. BCB ve CFV boyaları arasındaki derişim oranının, elde edilen spektruma yansıdığı gözlemlenmiştir. Gömülme çalışmasında kullanılan boyaların derişim oranı ile sinyal yoğunlukları oranı arasında doğrusal bir ilişki bulunmuştur.

Anahtar Kelimeler: Nanoparçacık, nano etiket, yüzeyde güçlendirilmiş Raman spektroskopisi, tek boya yüklü nano etiket, çoklu boya yüklü nano etiket, çoklu analiz.

To my little three girl, mom and two sisters, and to dad…

ACKNOWLEDGEMENTS

I would like to express my sincere thanks to my supervisor Prof. Dr. Mürvet Volkan not only for her guidance, support, encouragement, endless patience but also for listening and helping us in many ways of life. It was a great pleasure of mine to know her.

I wish to express my sincere gratitude to Assoc. Prof. Dr. Şeniz Özalp Yaman, Assoc. Prof. Dr. Belgin İşgör, Assoc. Prof. Dr. Atilla Cihaner and Assoc. Prof. Dr. Tirkeş in Atılım University for their valuable support, suggestions and understandings.

I would like to thank so much to Murat Kaya whose academic and moral support and advices help me grow my way of 'look'ing. I thank Seher Karabıçak for her support and help in Raman studies.

I am deeply grateful to Tacettin Öztürk, Ümit Zengin, Ufuk Özgen, Bahar Köksel and Burcu Küçük to make me find answers to the most challenging questions life asks. Thanks folks.

I would deeply like to thank Ceyhan Çiğdemoğlu, Doğanç Küçük, Tamer Çalışır, Engin Ayatar, Emine G. Cansu Ergün, Ümran Aydemir and Salih Ertan for making every second we shared a joyful story to tell and for their valuable smiles. My specials thanks are for Ozan Özkan for his support keeping me stand and making me smile even at the hardest times.

My special thanks go to my small but huge family, Sevim Kibar, Cemal Kibar, Sevda Kibar and Sümeyye Kibar for their loving me the way I am and for making me know that they are always on the next side of me regardless the kilometers and never leave me alone. Love brings you to me. Love does.

Barış! I am very glad you are here next to me with all your being making life a huge, colorful ocean. I thank you by my heart.

TABLE OF CONTENTS

LIST OF TABLES

TABLES

LIST OF FIGURES

FIGURES

LIST OF ABBREVATIONS

$Ag@SiO_2$	Silica coated Ag particles
$Ag\text{-}BCB@SiO_2$	BCB doped silica coated Ag nanotags
$Ag\text{-}BCB\text{-}CFV@SiO_2$	BCB and CFV doped silica coated Ag nanotags
$Ag\text{-}CFV@SiO_2$	CFV doped silica coated Ag nanotags
$Ag\text{-}CV@SiO_2$	CV doped silica coated Ag nanotags
ATP	4-aminothiophenol
BAD	bcl2-associated death promoter
BAX	bcl2-associated X protein
BCB	Brilliant cresyl blue
BMBA	2-bromo-4-mercaptobenzoicacid
CFV	Cresyl fast violet
CV	Cresyl violet
DTDC	3,3'-diethylthiadicarbocyanine iodide
DTNB	5,5'-dithiobis (2-nitrobenzoic acid)
Eu-TDPA	Tris(dibenzoylmethane) mono(5-aminophenanthroline)europium
EDX	Energy dispersive X-ray spectrometry
FE-SEM	Field emission scanning electron microscopy
FITC	Fluorescein isothiocyanate
LUMO	Lowest unoccupied molecular orbital
MBA	4-mercaptobenzoic acid
MEF	Metal enhanced fluorescence
MGITC	Malachite green isothiocyanate
MT	4-mercaptotoluene
NNI	National Nanotechnology Initiative
PMAA	Polymethacrylic acid
QD	Quantum dot

RB	Rhodamine B
Rh800	Rhodamine 800
Rubpy	Tris(2,2’-bipyridyl)-dichlororuthenium (II) hexahydrate
R6G	Rhodamine 6G
SERS	Surface enhanced Raman scattering
TEOS	Tetraethoxysilane
TMR	TAMRA
TRITC	Tetramethylrhodamine-5-isothiocyanate
XRITC	X-rhodamine-5-(and-6)-isothiocyanate
6-FAM	6-carboxyfluorescein

CHAPTER 1

INTRODUCTION

1.1 Tagging

With the wish of knowing and controlling the locality, man, the most advanced and developed of all other species tends to understand the lower organisms, so 'inside' and so surroundings. Going through the way of understanding and treatment of living and thinking systems in this endless quest, recent search on biosystems has focused on the qualification, quantification and localization of specific biomolecules. Due to the difficulty of direct detection of biomolecules at trace amounts, innovation and invention of so called-tags made an era in chemistry and molecular biology.

Tags are materials used for signing substances and so make possible the qualitative and quantitative analysis both in macroscopic and microscopic world. On this basis, fluorescence spectroscopy is one the most used techniques among the optical based-tag detection systems and organic fluorophores have been widely used to detect compounds in trace levels [1].

Fluorophore can be a molecule or a functional organic group absorbing light at particular wavelength, emitting light at other specific wavelength. The wavelength of the emitted radiation can be controlled by the chemical nature of the organic dye [1, 2]. Fluorophores have generally high quantum yield and are versatile and ease to use [3, 4]. On the other hand, they suffer from some important drawbacks. They are not

photostable in the case of long exposure to light, photobleach, have broad emission spectra and short emission lifetimes and also give irreproducible results due to false-positive or false-negative signals resulting from degradation [3, 5, 6]. Toxicity is one other important problem hindering their applications for *in vivo* cellular studies [4]. In addition, biomolecules, like DNA probes can be labeled with only one or a few fluorophores [6]. Hence, in the case of low concentration for target, the low signal amplification of fluorophores results in the too weak signals to be detected and so in the failure of targeting biological molecules [1, 3]. These limitations of fluorophores gain much more importance during the usage of nanoparticles as labels in biological applications.

1.2 Nanoparticles

1.2.1 Nanotechnology

'But there's plenty of room at the bottom to make them smaller.' Richard Feynman [7].

Long before anything related with the word *nano* had emerged, in December 1959, history of nanotechnology took a start with the speech, titled as 'There's plenty of room at the bottom', by Physics Nobel Laureate Richard Feynman [7] for the American Physical Society at the California Institute of Technology in Pasadena. In that well-known lecture, he said 'I will not now discuss how we are going to do it, but only what is possible in principle' and explained what exciting opportunities would be bring up with learning how to control single atoms and molecules and improvements in the performance of instruments like electron microscopes, such as writing letters 25,000 times smaller than normal, so the entire content of *Encyclopaedia Britannica* on the head of a pin, making computer components having diameters of 10 to 100 atoms, modeling information systems on biological systems, manufacturing extremely small

devices and manipulating individual atoms. Despite Feynman, like anyone else, did not use the term ‘nanotechnology’, it is fair to say that this lecture was a vision of what is now called as nanotechnology [8].

National Nanotechnology Initiative (NNI) states that ‘Nanotechnology is the research and technology development at the atomic, molecular, or macromolecular scale, leading to the controlled creation and use of structures, devices, and systems with a length scale of 1–100 nanometers nm’. At this dimension, objects gain some novel properties and functions significantly different from those seen in the bulk scale. For example, carbon nanotubes and gold nanoshells have physical properties different from carbon or gold on the macro scale [9].

Nanometric studies have a wide spectrum of research areas and industrial activities from fundamental sciences that is physics, chemistry and biology to applied sciences, electronics and materials. Usage of nanoparticles is reported in a wide variety of areas [10]. Examples for industrial properties and applications of nanoparticles are given in Table 1.1 and 1.2, respectively.

Table 1.1 Examples for properties of nanoparticles in industry.

Property	**Nanoparticle**
Self-cleaning	SiO_2 [11], TiO_2 [12]
Anti-microbial	Ag [13], CuO [14]
Magnetic	γ-Fe_2O_3, Fe_3O_4 [15], Co [16]
Electrically conductive	SnO_2 [17], ATO [18]
UV-IR resistive	ITO [19], ZnO [20], CeO_2 [21]
Scratch resistive	ZrO_2 [22], Al_2O_3 [23], TiO_2 [24]
Fire retardant	Melamine cyanurate [25]
Water-repellent	SiO_2 [26, 27]

Table 1.2 Examples for applications of nanoparticles in industry.

Nanoparticle	**Application**
Al_2O_3, fullerene	Refrigeration [28, 29]
PbS, ZnO	Fuel cell [30], solar energy cells [31]
CuO, In_2O_3, SnO_2	Gas sensors [32, 33, 34]
Au, FePt	Data storage [35, 36]
Pd, Ni	Catalysis [37, 38]
Li containing oxides, Co_3O_4	Batteries [39, 40]
Ag, TiO_2	Cosmetics [41, 42]
SiO_2, Si_3N_4	Plastics [43, 44]
C, Ag	Water purification [45, 46]
$NiFe_2O_4$, $CoFe_2O_4$	Ferrofluids [47, 48]

1.2.2 Nanotechnology and Molecular Biology

Living organisms consist of cells of typically 10 µm across. The cell parts are much smaller, in the sub-micron size domain. Proteins are even smaller, having typical size of just 5 nm and this is comparable with the dimensions of smallest man-made nanoparticles. The relative dimensions of *things* [49] are presented in Figure 1.1.

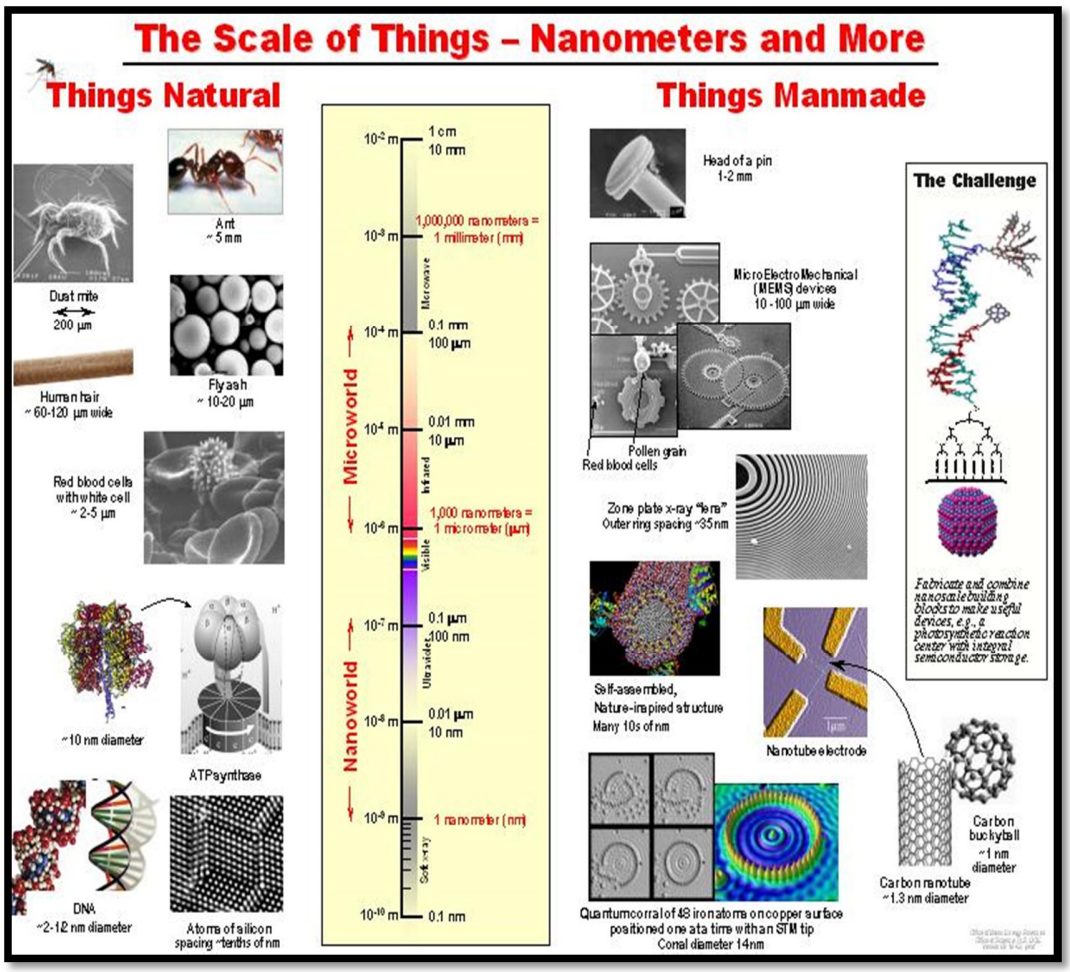

Figure 1.1 The scale of things [49].

This simple size comparison explains the principle beyond the usage of nanoparticles as very small probes for biotagging or labeling, making possible to spy at the cellular machinery [50]. In addition to their dimensional similarity, nanoparticles have also wide variety of important size dependent properties leading to many different biological applications. Examples for unique properties of common-use nanoparticles and for applications in molecular biology are given in Table 1.3 and Table 1.4, respectively.

Table 1.3 Examples for properties of nanoparticles in molecular biology.

Nanoparticle	**Characteristics**
Au	Stability, optical absorption, fluorescence and Raman scattering
Ag	Surface enhanced fluorescence, Surface enhanced Raman scattering
Pt	Catalytic property
CdSe	Luminescence, photostability
Fe_2O_3	Magnetic property
SiO_2	Biocompability

Table 1.4 Examples for applications of nanoparticles in molecular biology.

Application	**Nanoparticles**
Tissue engineering	Iron oxide [51]
Tumor-destroying hyperthermia	Au [52], iron oxide [53]
MIR contrast enhancement	Iron oxide [54], Gd [55]
Drug and gene delivery	Chitosan [56], Au [57]
Separation and purification	Iron oxide [58], Ni [59]
Detection of proteins	Au [60], Ag [61]
Detection of pathogens	Ag [62], Au [63]
Probing of DNA	Latex [64], Ag [65]
Phagokinetic tracking	Quantum Dots [66]

Due to the great utility they have in the area of molecular biology, also some companies started to interest in development and commercialization of nanoparticles and are listed in Table 1.5 [50].

Table 1.5 Examples for companies commercializing nanoparticles for bio and medical applications [50].

Company	Major area of activity	Technology
Advectus Life Sciences Inc.	Drug delivery	Polymeric nanoparticles engineered to carry anti-tumour drug across the blood-brain barrier
Alnis Biosciences, Inc.	Bio-pharmaceutical	Biodegradable polymeric nanoparticles for drug delivery
Argonide	Membrane filtration	Nanoporous ceramic materials for endotoxin filtration, orthopaedic and dental implants, DNA and protein separation
BASF	Toothpaste	Hydroxyapatite nanoparticles seems to improve dental surface
Biophan Technologies, Inc.	MRI shielding	Nanomagnetic/carbon composite materials to shield medical devices from RF fields
Capsulution NanoScience AG	Pharmaceutical coatings to improve solubility of drugs	Layer-by-layer poly-electrolyte coatings, 8–50 nm
Dynal Biotech		Magnetic beads
Eiffel Technologies	Drug delivery	Reducing size of the drug particles to 50–100 nm
EnviroSystems, Inc.	Surface desinfectsant	Nanoemulsions
Evident Technologies	Luminescent biomarkers	Semiconductor quantum dots with amine or carboxyl groups on the surface, emission from 350 to 2500 nm
Immunicon	Tarcking and separation of different cell types	magnetic core surrounded by a polymeric layer coated with antibodies for capturing cells
KES Science and Technology, Inc.	AiroCide filters	Nano-TiO2 to destroy airborne pathogens
NanoBio Cortporation	Pharmaceutical	Antimicrobal nano-emulsions
NanoCarrier Co., Ltd	Drug delivery	Micellar nanoparticles for encapsulation of drugs, proteins, DNA
NanoPharm AG	Drug delivery	Polybutilcyanoacrylate nanoparticles are coated with drugs and then with surfactant, can go across the blood-brain barrier
Nanoplex Technologies, Inc	Nanobarcodes for bioanalysis	
Nanoprobes, Inc.	Gold nanoparticles for biological markers	Gold nanoparticles bio-conjugates for TEM and/or fluorescent microscopy
Nanoshpere, Inc.	Gold biomarkers	DNA barcode attached to each nanoprobe for identification purposes, PCR is used to amplify the signal; also catalytic silver deposition to amplify the signal using surface plasmon resonance
NanoMed Pharmaceutical, Inc.	Drug delivery	Nanoparticles for drug delivery
Oxonica Ltd	Sunscreens	Doped transparent nanoparticles to effectively absorb harmful UV and convert it into heat
PSiVida Ltd	Tissue engineering, implants, drugs and gene delivery, bio-filtration	Exploiting material properties of nanostructured porous silicone
Smith & Nephew	Acticoat bandages	Nanocrystal silver is highly toxic to pathogenes
QuantumDot Corporation	Luminescent biomarkers	Bioconjugated semiconductor quantum dots

Using nanotags in biological applications can overcome the problems associated in the case of classical organic fluorophores. As an important incoming of nanotags, the possibility of encapsulation of more than one label inside a nanoparticle results in the

much more amplified signal than a single fluorophore does when conjugated to a biological molecule.

1.2.3 Nanotags

Nanotag systems making an era in trace analysis of biomolecules include fluorescence-based tags, so called the quantum dots, lanthanide nanoparticles, dye-doped silica nanoparticles, metal enhanced fluorescence, and Raman-based tags, namely Surface Enhance-Raman Scattering tags.

1.3 Fluorescence-Based Nanotags

1.3.1 Quantum Dots

Quantum dots, QDs are the most intriguing class of fluorescent probes. They are spherical semiconductors having diameters 1 and 10 nm. A typical QD is composed of atoms from Groups II-VI (CdSe, CdTe, CdS), III-V (InP, InS, ZnSe) or IV-VI (PbS, PbTe). However, Chan et al. [67] brought a new approach to preparation of QDs by coating CdSe cores with a layer of ZnS.

Over classical organic fluorophores, QDs have many advantages. They are stable in longer time than organic fluorescent dyes in the case of intense illumination and the fluorescence lifetime of QDs is orders of many multiples of typical organic dye lifetimes [1].

Despite these advantages, QDs suffer from some limitations for widespread use. Cytotoxicity is a definite concern for biological applications since the core is composed of toxic heavy metals like Cd [68]. They are insoluble in water and so surface modification is required for hydrophilicity [6]. In addition, blinking behavior, switching emission 'on' and 'off' by sudden stochastic jumps under continuous excitations, cause the failure in single particle tracking and raster scanning systems [3, 6].

1.3.2 Lanthanide Chelate and Lanthanide Doped Inorganic Compounds

Lanthanide nanoparticle group includes Eu^{+3}, Sm^{+3}, Tb^{+3} and Gd^{+3} [4]. In literature, actually, a limited number of studies present based on lanthanide nanoparticles usage as label and there mentioned two general approach in preparation differing in the usage of a chelate or not. For instance, Ye et al. [69] prepared silica coated-Eu+3 chelate, 4,4'-bis(1'',1'',1'',2'',2'',3'',3''-heptafluoro-4'',6''-hexanedion-6''-yl)cholorosulfo-*o*-terphenyl-Eu+3.

On the other hand, lanthanide doped inorganic nanoparticles consist of trivalent lanthanide ions, not chelates encapsulated with host matrices such as an oxide or fluoride. When compared to lanthanide chelates, lanthanide doped nanoparticles have longer fluorescence lifetime, up to several milliseconds, and higher photochemical stability [70]. Sivakumar et al. [71] studied the preparation of such kind of particles, silica coated Ln^{+3} doped LaF_3 nanoparticles.

Lanthanide based nanotags also have superior chemical and optical properties over organic fluorophores as having high quantum yields, sharp absorption and emission lines, high photostability and long fluorescence [72]. In addition, unlike QDs, lanthanide nanoparticles do not suffer from photobleaching, blinking and toxicity [4, 6].

1.3.3 Dye Doped Silica Nanoparticles

A typical dye doped-silica nanoparticles consists of dye molecules embedded into the silica sol gel network. Estèvez et al. [73] prepared FITC doped and tris(2,2'-bipyridyl)-dichlororuthenium (II) hexahydrate (Rubpy) doped silica nanoparticles.

Silica coating takes many advantages to the nanotag system. Such a layer prevents dye photobleaching, communication to the outside environment and dye leakage. Silica nanoparticles easily disperse in water and their surface can be modified easily to attach biomolecules through many existing molecular immobilization mechanisms [74]. When combined with excellent photostability and size uniformity and tunability, these nanotags provide high quality fluorescence signals [75].

1.3.4 Metal Enhanced Fluorescence Tags

Metal enhanced fluorescence, MEF tags are simply fluorophores being in contact with plasmon resonant particles. When fluorophore is placed within 4–10 nm of the surface of the plasmon nanostructures, the emission signal of that fluorophore is enhanced [76]. This enhancement effect can be explained in terms of changes in the photonic mode density, where a large mode density provides more radiation [77].

The superior advantage of metal enhanced fluorescence tags over dye doped silica coated nanoparticles was experimentally showed in one of the studies by Aslan et al. [78]. They prepared Tris(dibenzoylmethane) mono(5-amino phenanthroline) europium (Eu)-TDPA doped-Ag@SiO_2 and Rhodamine 800 (Rh800)-doped Ag@SiO_2 particles and also control sample probes including no silver cores. It was observed approximately 8-

fold and 20-fold higher for Eu-TDPA-doped Ag@SiO_2 and Rh800-doped Ag@SiO_2 than for Eu-TDPA-doped SiO_2 and Rh800-doped SiO_2.

1.4 Surface Enhanced Raman Scattering Tags

Surface enhanced Raman scattering, SERS tags are basically composed of Raman active molecule adsorbed on the roughened substrates or surfaces of metal nanoparticles such as Ag, Au, Cu, Li, Al, Na, and Fe [79]. SERS tags provides a combination of the unique fingerprint spectra of Raman spectroscopy, as well as many other advantages, with ultrasensitive detection limits provided by the enhancements due to the intense localized fields of metallic nanostructures .

1.4.1 Raman Spectroscopy

Raman spectroscopy is based on the radiation being scattered with a change in the incident photon frequency after coming in contact with matter and its history goes 80 years back. It was in 1928 that Indian scientist Sir Chandrasekhra Venkata Raman (Figure 1.2) discovered the scattering effect earning him a Nobel Prize in 1930 as a result of 9 years-study initiated by his observation on the color of the sky and Mediterranean Sea during a travel and published in 1922 [80].

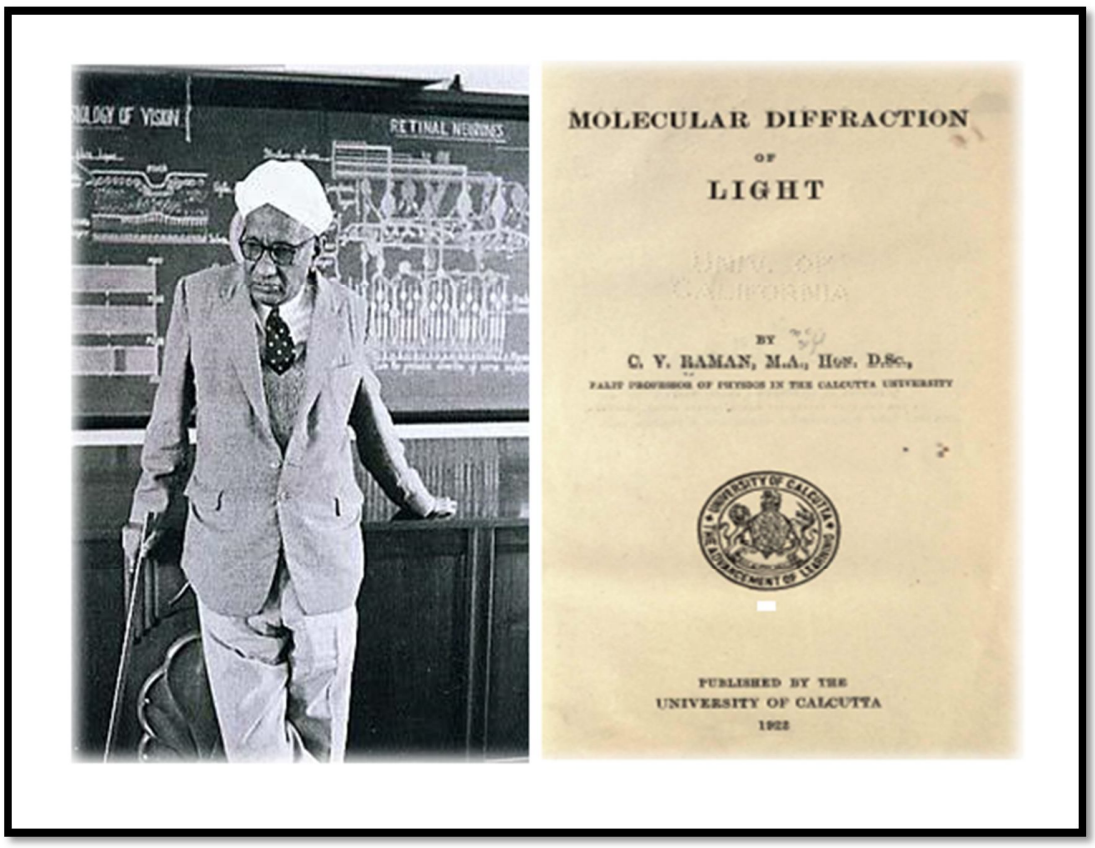

Figure 1.2 Indian scientist Sir Chandrasekhra Venkata Raman and the cover page of the study earning him the Noble Prize.

Raman effect can be described using the energy level diagram in Figure 1.3 [81]. When photon comes in contact with matter, the energy of the molecule raises from the ground state to a virtual state. Virtual states are not real states and created only when the laser interacts with the electrons and causes polarization [82]. After going up to the virtual state, the molecule immediately relaxes back to the original electronic state by emitting a photon.

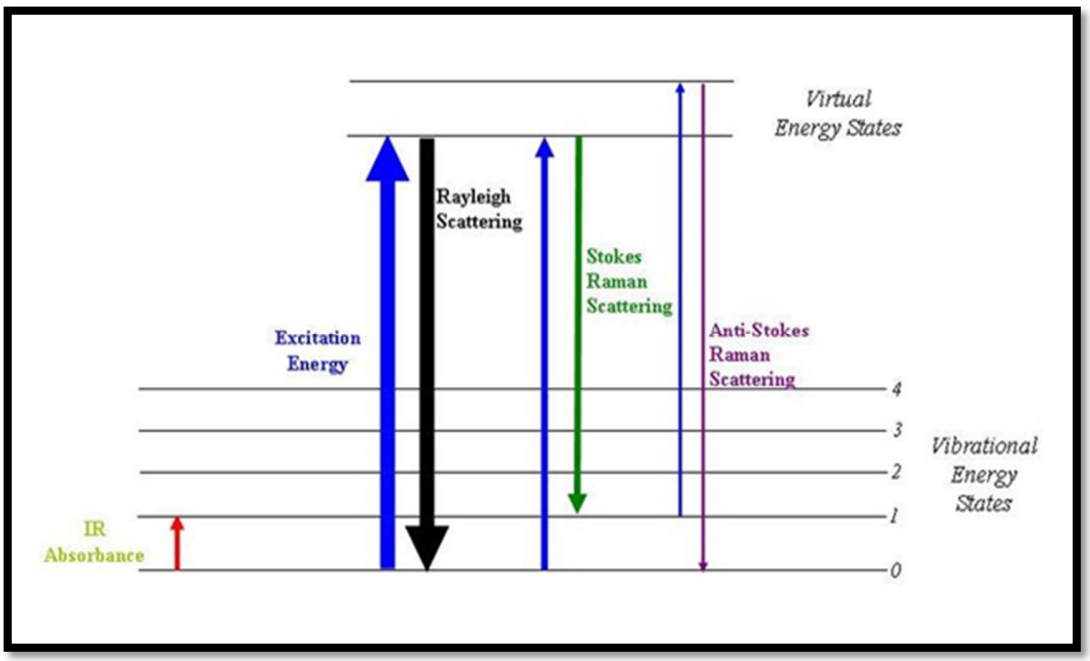

Figure 1.3 Energy level diagram [81].

If the scattered photon has the same frequency as the incident photon, this is Rayleigh scattering. On the other hand, if there is a change in the frequency of the incident photon, this scattering is called as Raman scattering and it may occur in two ways. If the scattered photon has less energy than the incident photon, this is Stokes Raman scattering and if the energy of scattered photon is more than the incident photon, then this is named as anti-Stokes Raman scattering [83].

The Stokes Raman intensity is proportional to the number of molecules in the lowest vibrational level whereas anti-Stokes Raman intensity is proportional to the number of molecules in the next higher vibrational energy level. Considering that at thermal equilibrium, the number of molecules in a lower vibrational energy level is always larger than the number of molecules in the next higher vibrational energy level, it is

clear that the Stokes Raman intensity will always be larger than the anti-Stokes Raman intensity. Hence, Raman scattering is usually assumed to be Stokes Raman scattering unless is labeled as anti-Stokes [84]

A Raman spectrum is a plot of scattered intensity as a function of difference in energy between the incident and scattered photons and this frequency difference between incident and Raman scattering light is termed the Raman shift, which is unique for individual molecules and is represented as cm^{-1} [85].

Raman spectroscopy has many advantages over other spectroscopic techniques. The spectra are specific to the scattering molecule, giving high information content. Water, the most common solvent in biological studies, is a weak scatterer, eliminating a potential interference. Since the frequency of Raman scattered photons is a fixed shift on the energy of the exciting photon. In the case of a spectral interference, it is possible to change the excitation wavelength leading to moving the wavelength of the scattered photons into a different frequency region. On the other hand, the Raman scattering process occurs with low probability, compared to most fluorescence events, resulting in very few detectable photons and so weak signals. Because of the last factor, it is difficult to measure low concentrations of species directly by traditional Raman scattering [86].

1.4.2 Surface Enhanced Raman Spectroscopy

In 1974, the discovery of Fleischmann et al. [87] based on the unexpectedly high Raman signals from pyridine on a silver electrode roughened with oxidation-reduction cycles attracted considerable attention. By the time, it was predicted that the intense signal is from the larger surface area of the metal electrode interacting with molecules. Then, in 1977, Albrecht et al. [88] figured out that larger active area alone could not account the

enhancement in signal and there must be a true enhancement of the Raman scattering efficiency itself for enormously strong intensity in pyridine on a rough silver electrode [89]. Role of surface plasmon resonance in enhancement was experimentally proved in 1985 [90]. In the time interval between the mid-1970s and the early 1980s, SERS could not make big steps in practical meaning due to observed enhancement for only a limited number of molecules, mostly pyridine [79]. In 1984, the general applicability of SERS as an analytical technique was first illustrated by Vo-Dinh et al. [91] using silver spheres-coated substrates for trace organic analysis. This approved enhancement in Raman signal in the presence of metal nanoparticles showed promise to overcome the traditionally low sensitivity problem in Raman spectroscopy [92].

1.4.3 SERS Effect

There are two commonly considered mechanisms for SERS, one of which involves enhancements in the field intensity as a result of plasmon resonance excitation and the other the enhancement in polarizability due to chemical effects [93]. A schematic of normal and surface enhanced Raman scattering is presented in Figure 1.3.

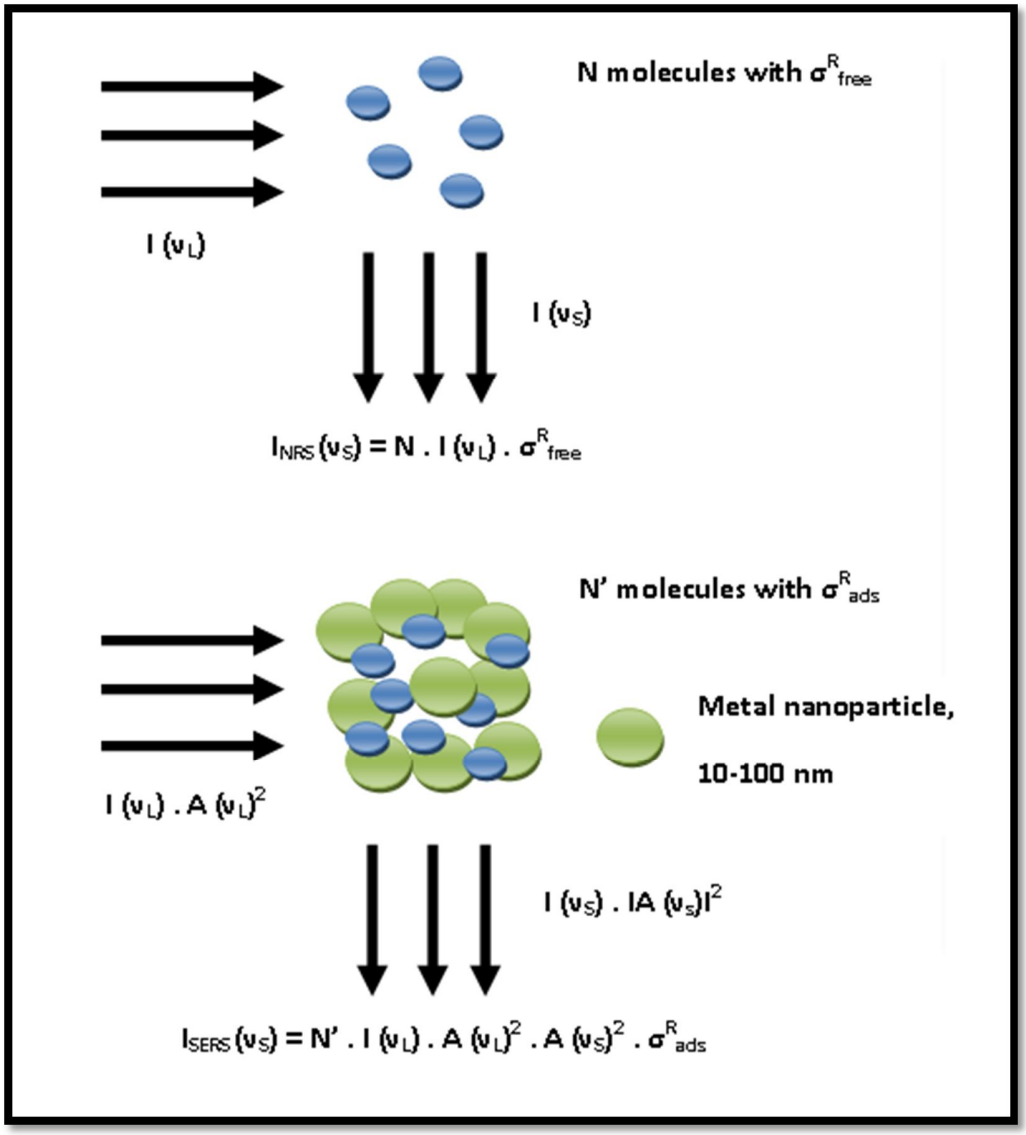

Figure 1.4 The normal scattering and surface enhanced Raman scattering [89].

In normal Raman scattering, the total Stokes Raman signal I_{NRS} is proportional to the Raman cross section σ^R_{free}, the excitation laser intensity $I_{(\nu L)}$, and the number of molecules N in the probed volume. On the other hand, in the case of the Surface enhanced Raman scattering, the signal I_{SERS} is proportional to the increased Raman

cross section of the adsorbed molecule σ^{R}_{ads}, the excitation laser intensity $I_{(\nu L)}$, and the number of molecules which are involved in the SERS process N'. There, σ^{R}_{ads} describes the chemical enhancement and $A_{(\nu L)}$ and $A_{(\nu S)}$ are the field enhancement factors [89]. It was explained that the chemical enhancement contribution is much smaller, in the order of 10^2-10^3, when compared to the contribution of electromagnetic enhancement which is on the order of 10^{11} [94].

1.4.3.1 Electromagnetic Enhancement

When a small spherical metallic nanoparticle is irradiated by light, the oscillating electric field leads to the displacement of the conduction electron charge cloud relative to the nuclei with the passage of the wave front, so-called coherent oscillation of conduction electrons [95]. The collective excitation of the electron gas of a conductor is called a plasmon and if the excitation is confined to the near surface region it is called a surface plasmon [96].

Electromagnetic field effect is arising from these exciting localized surface plasmons of the metal nanoparticles. An intense light scattering appears when the monochromatic light is resonant to the surface plasmon of particle. That scattered light is characterized by an electromagnetic field intensity which is extremely strong at a fixed space near the nanoparticle surface. A molecule present in that space is excited by an enhanced field and produces more intense Raman scattered light than molecules outside that space. In addition, the scattered light can excite the surface plasmons of nanoparticles in the case of low wavenumber shifts. Hence, the plasmon reemits light having Raman shifted wavelength with an additional enhancement [97].

1.4.3.2 Chemical Enhancement

Chemical enhancement is another mechanism that is responsible for the SERS effect, in which the Raman polarizability of a molecule adsorbed on a metal surface is enhanced and charge transfer mostly contributes [98]. This electronic coupling between molecule and metal leads to an increased Raman cross section of the adsorbed molecule in the complex compared with the cross section of a free molecule in a normal Raman experiment [92]. Possible electronic SERS mechanisms involve a resonance Raman effect due to a new metal-molecule charge-transfer electronic transition or a dynamic charge transfer between the metal and molecule [98].

1.4.4 SERS Tags over Fluorescence Tags

Raman tags possess many advantages such as yielding unique spectrum for each Raman reporter, being excited at any wavelength, not suffering from photobleaching and having high sensitivity [99, 100, 101]. As a very important point, whereas fluorophores have broad peaks of 50-70 nm, Raman emission is characterized by narrow peaks of nearly 2 nm [102]. Fluorescence has the disadvantage that the spectra produced tend to have broad overlapping spectra thus the multiplexing capacity of the technique is limited [103]. On the other hand, very narrow peak widths Raman yields provide a structural fingerprint of molecule and also prevent overlapping of peaks belonging to different molecules [92, 101].

SERS have comparable sensitivity but a higher selectivity due to the Raman fingerprint region, in which the peaks are narrower and more easily resolved, when compared to fluorescence. This allows the detection of multiple labels, in highly multiplexed assays, with SERS tags to a degree not possible with fluorescence [104].

1.4.5 Preparation of SERS Tags

In literature, there are basically two approaches to prepare SERS nanotags. One method is based on the direct attachment of the biomolecule labeled with Raman reporter to the nanoparticle probe. Cao et al. [105] prepared such kind of nanotags using gold nanotags for six different Raman active dyes-labeled oligonucleotides.

As a very important drawback, in this kind of tags, biomolecule is labeled with only one Raman reporter molecule and this makes trace analysis of biological compounds harder. In addition, in the absent of a layer, dye molecules become undefensive against the environmental conditions and so instable.

The other method to prepare SERS tags considers the synthesis of core/shell nanoparticles into which Raman active molecules embedded. Liu et al. [106] designed dye embedded core/shell Raman tags using both Ag and Au nanoparticles. After labeling of prepared nanoparticles with different dye molecules, tetramethylrhodamine-5-isothiocyanate (TRITC), 5,5'-dithiobis (2-nitrobenzoic acid)(DTNB) and FITC, silica was coated.

In this type of nanotags, the surface enhanced Raman signals reported do not come from the target molecules labeled with only one reporter molecule, but from many individual dye molecules that are embedded in the core-shell structure. Such a design overcomes the problems of poor data reproducibility [107]. In addition, a hydrophilic shell makes organic dyes easily suspended in water, which are generally insoluble and cannot uniformly dispersed in water [108].

Then, an efficient SERS tags mainly consist of three parts, as indicated in Figure 1.4, core nanoparticle for amplify the Raman signal, dye molecule for spectral signature and a shell layer for protection.

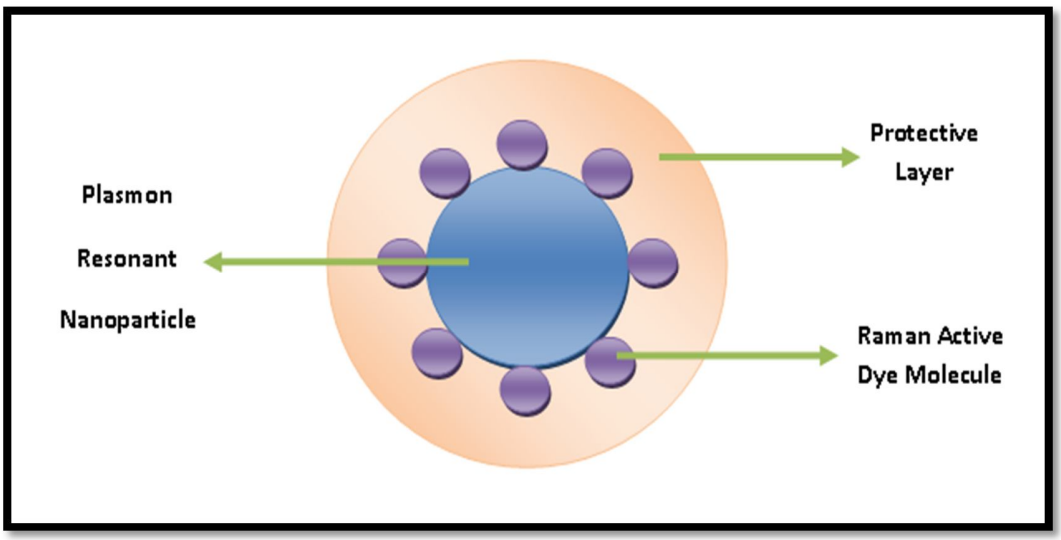

Figure 1.5 Components of an ideal SERS nanotag.

1.4.5.1 Core Nanoparticles

The most contribution to the SERS enhancement comes from the intense localized fields by plasmon resonant nanoparticles such as Au, Ag, Cu, Li, Al, Na, and Fe with sizes on the order of tens of nanometers [79]. However, for substantial SERS effect, metals such as Ag, Au and Cu should be used as core nanoparticles [109]. In addition, between these metals, the SERS enhancement of silver exceeds that of gold, which exceeds that of copper [110].

In literature, there are many procedures recorded for the preparation of Ag nanoparticles and some examples are given in Table 1.6. Among them, reduction by borohydride and citrate are the most applied methods due to the better enhancement effect and particle stability [111].

Table 1.6 Examples for the preparation techniques of Ag nanoparticles.

Preparation Technique	**Starting material**
Chemical Reduction by sodium citrate [112]	$AgNO_3$
by borohydride [113]	$AgNO_3$
by hydroxylamine [114]	$AgNO_3$
by hydrogen [115]	$AgClO_4$
Microwave plasma synthesis [116]	Ag_2CO_3
Rapid expansion of supercritical solvents [117]	$AgNO_3$
Microemulsion, [118]	$AgNO_3$
UV-reduction, [119]	$AgNO_3$
Laser ablation, [120]	Ag foil
Electrolysis, [121]	$AgNO_3$
Sonoelectrochemical, [122]	$AgNO_3$

1.4.5.2 Raman Active Dye Molecules

On the basis of conjugation of dye molecules to the nanoparticles, there are two optional approaches. The first way considers the formation of a covalent bond between the nanoparticles and dye molecules. Here, for such kind of interaction, dye should possess multisulfur or isothiocyanate groups. Doering et al. [107] performed such an encapsulation study with nanogolds using 3,3'-diethylthiadicarbocyanine iodide (DTDC), malachite green isothiocyanate (MGITC), TRITC, X-rhodamine-5-(and-6)-isothiocyanate (XRITC).

As a second way, encapsulation can be achieved using electrostatic interaction between nanoparticles and dye molecules. Then, in the case of the negatively charged Ag or Au particles, dye to dope should carry a positive charge. Gong et al. prepared dye embedded-silica coated Au tags using positively charged dyes, CV, R6G, rhodamine B (RB) in addition to 2-mercaptopyridine [99].

1.4.5.3 Protective Shell

The coating materials most often used have been an organic polymer or silica. The most common polymer matrices are polystyrene, polymethacrylic acid (PMAA), polylactic acid and polylactic-copolyglycolic acid [3]. Although they are well-used, polymer particles are hydrophobic, tend to agglomerate in aqueous medium and swell in organic solvents resulting in the dye leakage. Over polymer nanoparticles, there are several advantages of silica shells. Silica nanoparticles are easy to separate via centrifugation during particle preparation, surface modification and other solution treatment processes because of the higher density of silica (1.96 $g.ml^{-3}$ for silica and 1.05 $g.ml^{-3}$ for polystyrene). Silica nanoparticles are more hydrophilic and biocompatible, they are inert and not subject to microbial attack, and no swelling or porosity change occurs with the change in pH [3, 123]. Silica shell is optically transparent, so that chemical reactions can be monitored spectroscopically. The shell can also be used to modulate the position and the intensity of colloidal metal surface Plasmon absorption bands, which is the color of the metal sol. [124]

Silica shells are prepared by two general synthetic routes: microemulsion and Stöber processes. Water-in-oil microemulsion is an isotropic, thermodynamically stable and transparent solution consisting of water, oil and surfactant. In this system, the water nanodroplets behave like nanoreactors where synthesis of nanoparticles takes place [125]. The drawback of this method is usage of surfactant of which removal requires

additional troublesome washing steps. On the other hand, in 1968, Stöber [126] described a method for synthesis of silica nanoparticles, called as Stöber method. The system includes water and organic solvent and does not require surfactant.

Both silica layer formation procedures mainly depend on the hydrolysis and condensation of a silica precursor and TEOS is the most used one. The process involves basically, in the case of the citrate-stabilized Au or Ag nanoparticles, reaction of nanoparticles with hydroxyl groups TEOS to form covalently bound surface monolayer, further hydrolysis of the residual ethoxy groups of the silica thin film in the presence of water and a catalyst, reproduction of a uniform hydroxyl surface after each hydrolysis procedure. The silica shell growth is achieved by repetition of saturated adsorption of TEOS and subsequent regeneration of a uniform hydroxyl surface [99].

1.4.6 Recent SERS Studies

As a result of increase in biological understanding, there are now many opportunities to extract information on cellular and molecular processes from biological specimens [127]. Recently, the biomedical research community realized that single target-detection systems are no likely to provide enough information for characterization or detection of a specific disease process. [128]. The development of multiplexed tags has been driven by this need for sensitive and simultaneous detection of various trace biomarkers in a single assay [123, 129]. Compared to single dye-doped nanotags detection, multiplex analysis reduce the time, cost and sample volume required per analysis, allow for simpler assay protocols, facilitates interpretation of signals with non-uniform distribution throughout the specimen and give the opportunity of making comparison of samples feasible and measurements reproducible and reliable. Hence, multiplex assays are crucial to complement advances in genomics to allow a large number of nucleic acids to be rapidly screened [130, 127]. On this basis, commonly

used fluorescent tags suffer from significant limitations in multiplexing applications, such as autofluorescence interference from tissue and the overlapping of emission peaks. On the opposite hand, SERS tags exhibit unique spectral signatures with narrow peaks that are ideal for multiplexing [127]. In preparation of multiplex tags, type of dyes and the stoichiometry between them are two important parameters and the combination of these two results in the generation of very large number distinct SERS labels [131].

The ability to simultaneously detect multiple targets, sensitively and in vivo, is an attractive feat; but it is a task often difficult to accomplish [128]. In the limited number of researches in the literature, there are three common approaches in multiplex SERS tag preparation, i. conjugation of different biological molecules with different labels and then being combined with nanoparticles [105, 132, 133, 134], ii. conjugation of nanoparticles with each label separately to form single-component nanotags [135, 136] and coated with polymer [137] or with silica [138], and iii. conjugation of nanoparticles with solutions of Raman active molecules mixed at various ratios to form multi-component nanotags [139, 131].

CHAPTER 2

EXPERIMENTAL

2.1 Chemicals and Reagents

i. **Deionized water,** Millipore Milli-Q water system with the Millipore Elix 5 electro deionization system.

ii. **Silver Nitrate, $AgNO_3$,** ≥ 99.0 %, Sigma-Aldrich.

iii. **Sodium citrate tribasic dehydrate, $Na_3C_6H_5O_7.2H_2O$**, Sigma Aldrich. 1% solution was prepared using deionized water.

iv. **Tetraethoxysilane**, **$SiC_8H_{20}O_4$,** 98 %, Sigma Aldrich.

v. **Ethyl alcohol, C_2H_5OH,** Merck.

vi. **Isopropyl alcohol, C_3H_7OH,** 99.5 %, Birpa.

vii. **Ammonia, $NH_3.H_2O$,** 25 %, Merck.

viii. **Brilliant cresyl blue, $C_{17}H_{20}ClN_3O$,** Sigma Aldrich. 10^{-2} M stock solution was prepared using ethyl alcohol.

ix. **Cresyl fast violet, $C_{18}H_{15}N_3O_3$,** Sigma. 10^{-2} M stock solution was prepared using ethyl alcohol.

x. **Cresyl violet, $C_{25}H_{30}N_3Cl$,** Sigma Aldrich. 10^{-2} M stock solution was prepared using ethyl alcohol.

2.2 Instrumentation

2.2.1 Centrifugation

To remove unreacted species in the reaction medium, after each experimental procedure, product was collected, separated and washed two times with ethanol-water solution (5:4) and one additional time with water via centrifugation for 15 min at 5000 rpm using a centrifuger purchased from NÜVE, Turkey, and redispersed in water.

2.2.2 Field Emission Scanning Electron Microscopy

Surface morphology and particle size of particles prepared were determined with the help of a Quanta 400 F obtained from FEI Company, the Netherlands at METU Central Laboratory. The obtained products were dispersed in water and 25 µl of these solutions was dropped on the carbon tapes. After natural drying, characterization studies were performed at ambient conditions. Average arithmetic diameter and standard deviation were calculated for 40 particles selected randomly on the related Field Emission Scanning Electron Microscopy (FE-SEM) images.

2.2.3 UV-VIS Spectrometer

The optical properties of prepared samples were investigated using a T80 double beam UV-vis spectroscopy with a socket deuterium and tungsten halogen lamp and multiplier detector, purchased from PG Instruments, UK. The spectra of the diluted colloidal solution were recorded at room temperature.

2.2.4 Raman Spectroscopy

SERS measurements were performed with LabRAM HR confocal microscopy Raman Spectroscopy with a charge-coupled device detector and a holographic notch filter, obtained from Jobin Yvon LabRam. 632.8-nm radiation was applied for SERS excitation with the help of a He-Ne laser with a total power of 20 mW. The spectrometer was equipped with a 1800-grooves/mm grating. Entrance slit was 200-μm during all measurements. After washing steps, dye-doped particles were redispersed in 2 ml water. 25 µl of this dispersion was taken, dropped on a glass slide and left to dry for Raman measurements. Acquisition time was 1 s unless otherwise is told.

2.3 Procedure

2.3.1 Synthesis of Ag Particles

Ag nanoparticles were synthesized through Lee-Meisel procedure [140] based on chemical reduction by citrate. In a typical reaction (Figure 2.1), 90 mg $AgNO_3$ was dissolved in 500 ml of deionized water and left to boil. Afterwards, 10 ml of 1% sodium citrate solution were quickly added to this solution under magnetic stirring. Boiling was continued for an additional 1 hour. During this time, the colorless solution turned first to yellow and then to green. This resulting green Ag colloid solution was allowed to cool down to room temperature under stirring. The colloid solution was stored at dark at room temperature for further examinations.

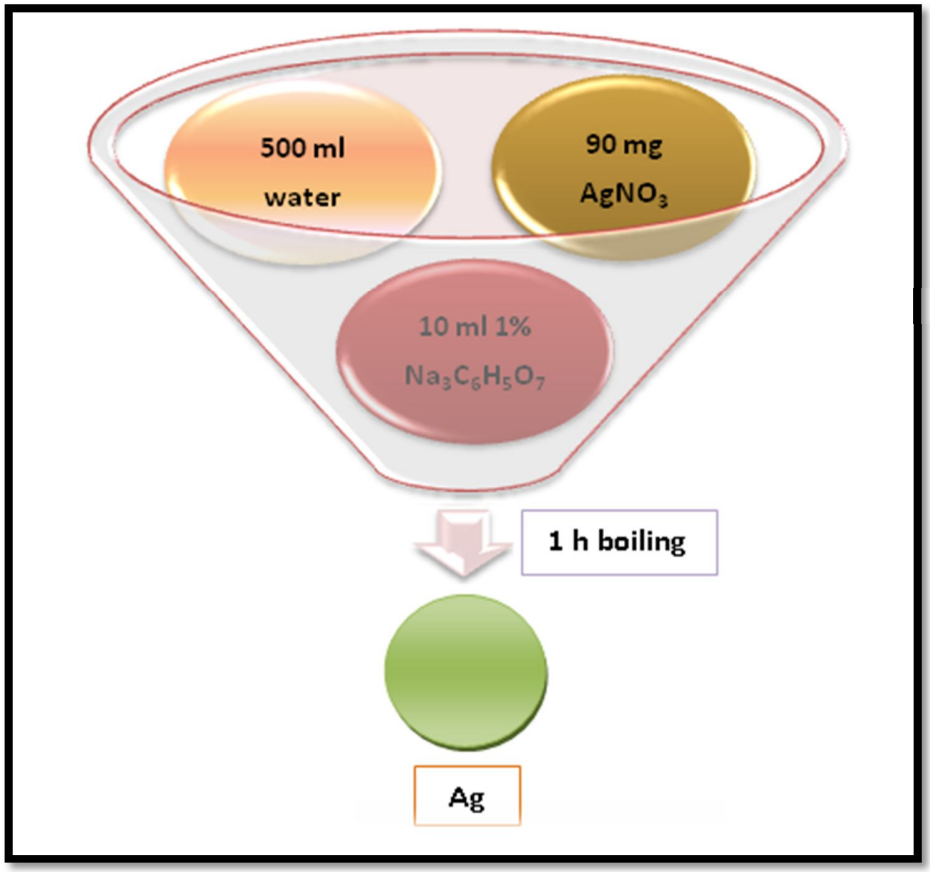

Figure 2.1 Preparation of Ag colloids using citrate reduction method.

2.3.2 Preparation of $Ag@SiO_2$ Particles

To determine a suitable experimental procedure, two different methods, both basing on Stöber process [126] were carried out. Molar ratio of TEOS to water, [TEOS]/[water] was studied to see the effect of amount of TEOS on coating.

2.3.2.1 Deposition Technique

In procedure A (Figure 2.2), Ag colloids were dispersed in 50 ml of ethanol-water solution (4:1). To this suspension, TEOS was added so that [TEOS]/[water] is $2x10^{-4}$ and 6.7 ml of ammonia were rapidly injected. The reaction proceeded for 12 hours.

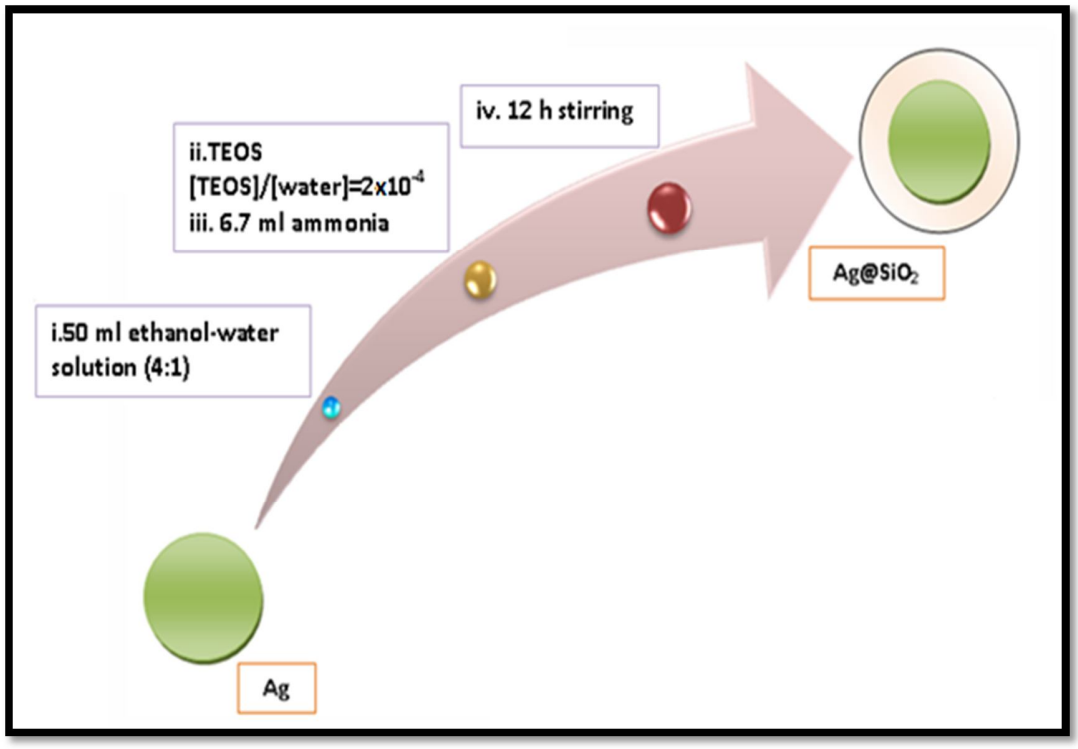

Figure 2.2 Procedure A applied for silica layer deposition on Ag nanoparticles.

In procedure B (Figure 2.3), to 50 ml of isopropanol-water solution (10:1) involving Ag colloids, same amount of TEOS ([TEOS]/[water]=$2x10^{-4}$) and ammonia (6.7 ml) were added. This mixture was left at room temperature for 30 min under magnetic stirring at room temperature and then kept at 4^0C for 20 hours.

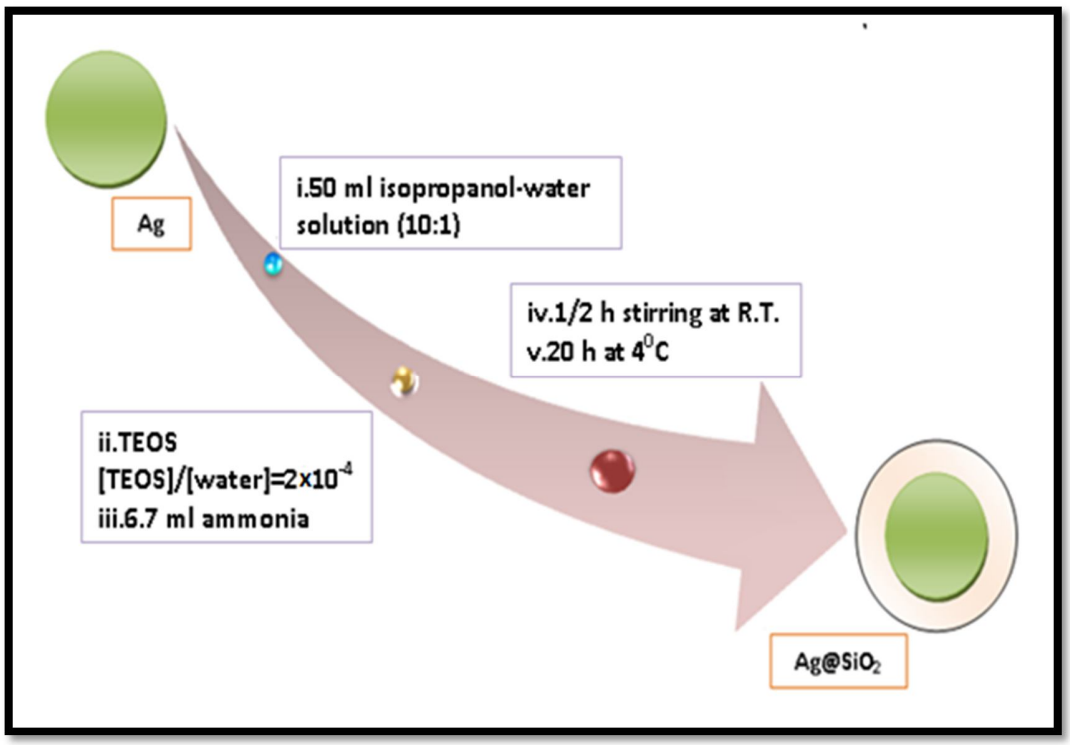

Figure 2.3 Procedure B applied for silica layer deposition on Ag nanoparticles.

2.3.2.2 Effect of [TEOS]/[Water] on Silica Thickness

Amount of TEOS is an important parameter affecting the silica layer thickness formed around the particles. In Procedure A, to the dispersion of Ag colloids in 50 ml ethanol-water solution (4:1), TEOS was added to adjust [TEOS]/[water] as $6x10^{-4}$, $2x10^{-4}$, $1x10^{-4}$, $9x10^{-5}$, $8x10^{-5}$ and $7x10^{-5}$. After addition of 6.7 ml ammonia, the mixture was left to react for 12 hours (Figure 2.4).

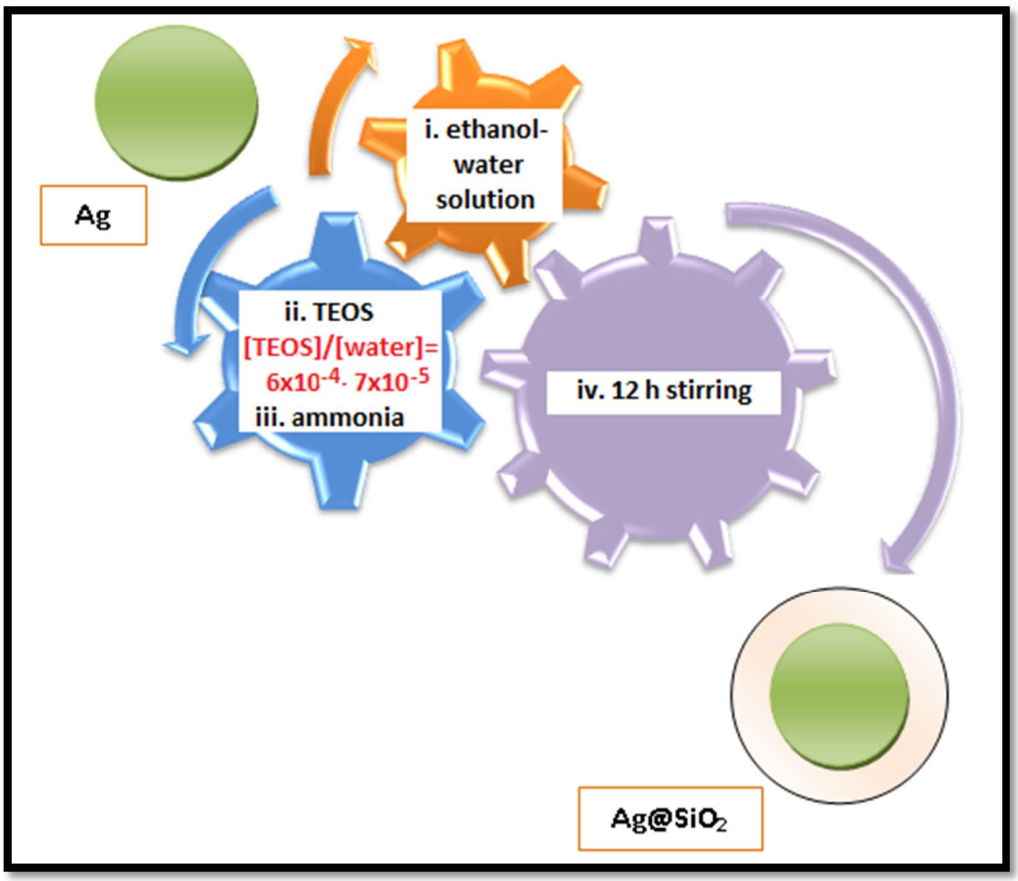

Figure 2.4 Silica layer deposition by varying [TEOS]/[water] from $6x10^{-4}$ to $7x10^{-5}$ in Procedure A.

2.3.3 Preparation of A Single-Dye Doped SERS Nanotag, Ag-BCB@SiO_2

2.3.3.1 Encapsulation Method

For encapsulation of BCB in silica coating layer, two approaches, namely impregnation and embedding were examined. In the case of the impregnation method (Figure 2.5), silica coated silver nanoparticles, prepared using Procedure A with [TEOS]/[water]=$9x10^{-5}$ and ammonia, were introduced into a 50 ml water-ethanol

solution (1:1). After obtaining a suspension through mixing, 500 µl of 10^{-2} M BCB solution were added, following by 12 hours magnetic stirring at room temperature.

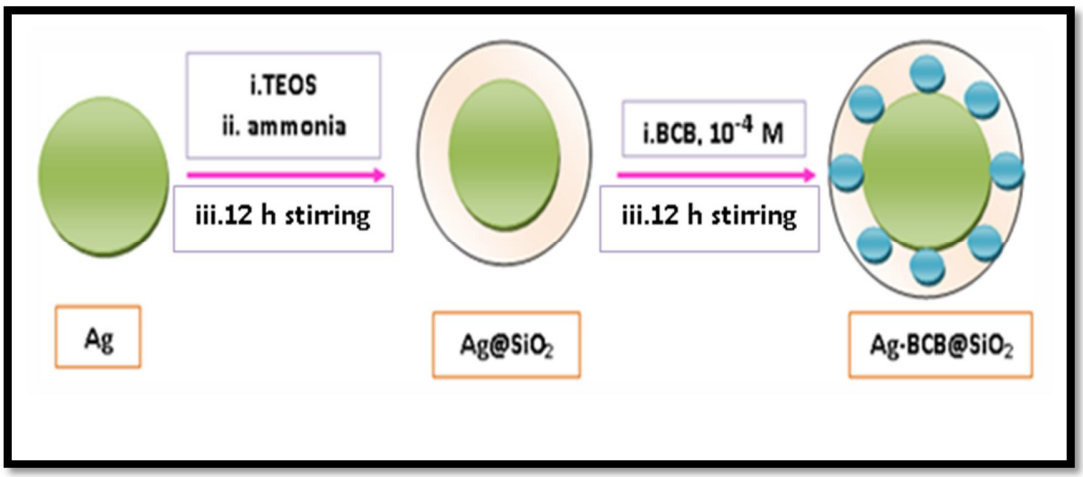

Figure 2.5 Preparation of Ag-BCB@SiO_2 nanotags using the impregnation method for $[BCB]_{rxn}$ is 10^{-4} M and [TEOS]/[water] is $9x10^{-5}$.

In the embedding method (Figure 2.6), bare silver nanoparticles were dispersed in a 50 mL ethanol-water solution (4:1) and same amount of BCB solution as in impregnation, 500 µl of 10^{-2} M BCB were added to the suspension. The mixture was left to stirring for 30 min for conjugation. Afterwards, the Procedure A involving [TEOS]/[water]=$9x10^{-5}$ and ammonia as catalyst was applied for silica deposition.

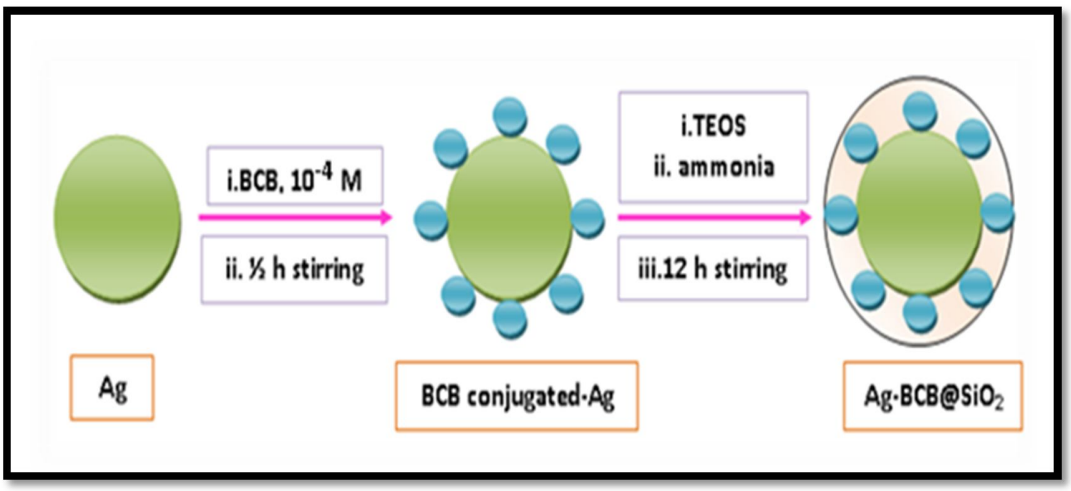

Figure 2.6 Preparation of Ag-BCB@SiO_2 nanotags using the embedding method for $[BCB]_{rxn}$ is 10^{-4} M and [TEOS]/[water] is $9x10^{-5}$.

2.3.3.2 Effect of Various Silica Thickness on Encapsulation

Through the embedding method, Ag colloids were treated with 500 µl of 10^{-2} M BCB for 30 min. To adjust different silica thicknesses, molar ratio [TEOS]/[water] was varied from $6x10^{-4}$ to $8x10^{-5}$ by changing the amount of TEOS added. After rapid injection of ammonia, the reaction proceeded for 12 hours under stirring (Figure 2.7).

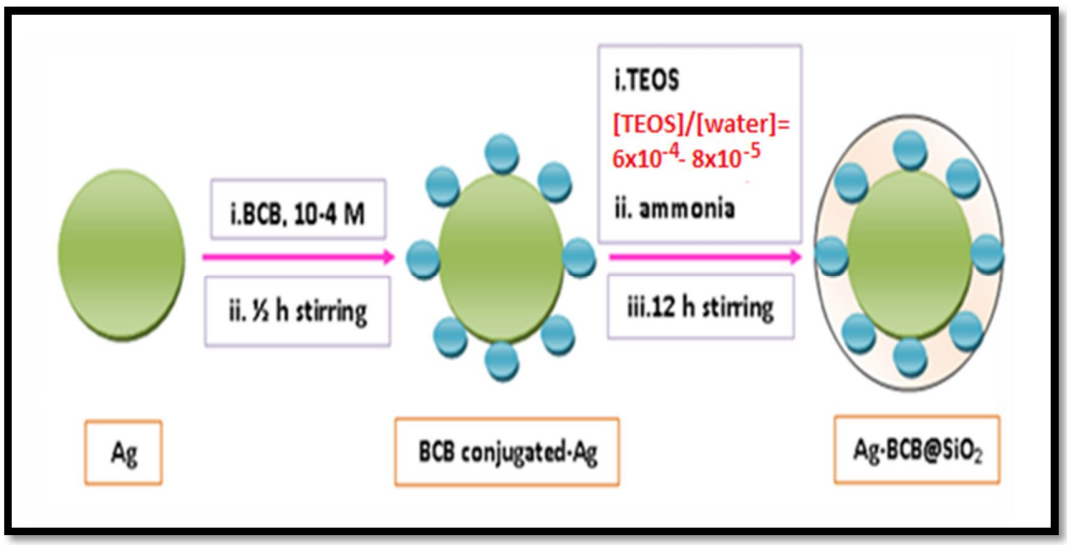

Figure 2.7 Preparation of Ag-BCB@SiO_2 nanotags by varying [TEOS]/[water] from $6x10^{-4}$ to $8x10^{-5}$ in the embedding method.

2.3.3.3 Effect of Total Dye Concentration on Encapsulation

The effect of change in the concentration of BCB in the reaction medium on the resulting product signal was examined. In the embedding method (Figure 2.8), BCB solutions were added to the ethanol-water solution involving Ag colloids, so that total dye concentration was $5x10^{-5}$, 10^{-4} and 10^{-3} M. After addition of TEOS ([TEOS]/[water]= $9x10^{-5}$) and ammonia, the reaction was continued for 12 hours under stirring.

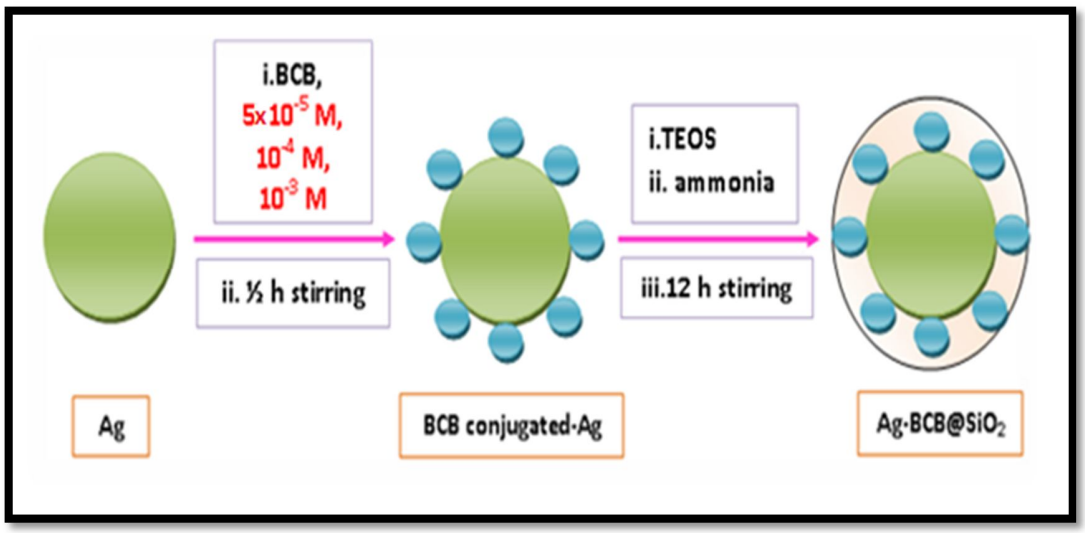

Figure 2.8 Preparation of Ag-BCB@SiO_2 nanotags by varying $[BCB]_{rxn}$ from $5x10^{-5}$ to 10^{-3} M in the embedding method.

2.3.4 Preparation of Different Single-Dye Doped SERS Nanotags, Ag-CFV@SiO_2 and Ag-CV@SiO_2 for Multiplex Analysis

CFV and CV were chosen as Raman active molecules to dope due to being positively charged like BCB. For preparation of CFV doped and CV doped nanotags, Ag-CFV@SiO_2 and Ag-CV@ SiO_2, embedding approach was followed. In a typical experiment, Ag colloids were allowed to be conjugated to CFV or CV in ethanol-water solution where total dye concentration was 10^{-3} M. After 30 min, TEOS was added to adjust [TEOS]/[water] as $9x10^{-5}$. Ammonia was rapidly injected and the reaction was left for 12 hours on stirrer (Figure 2.9).

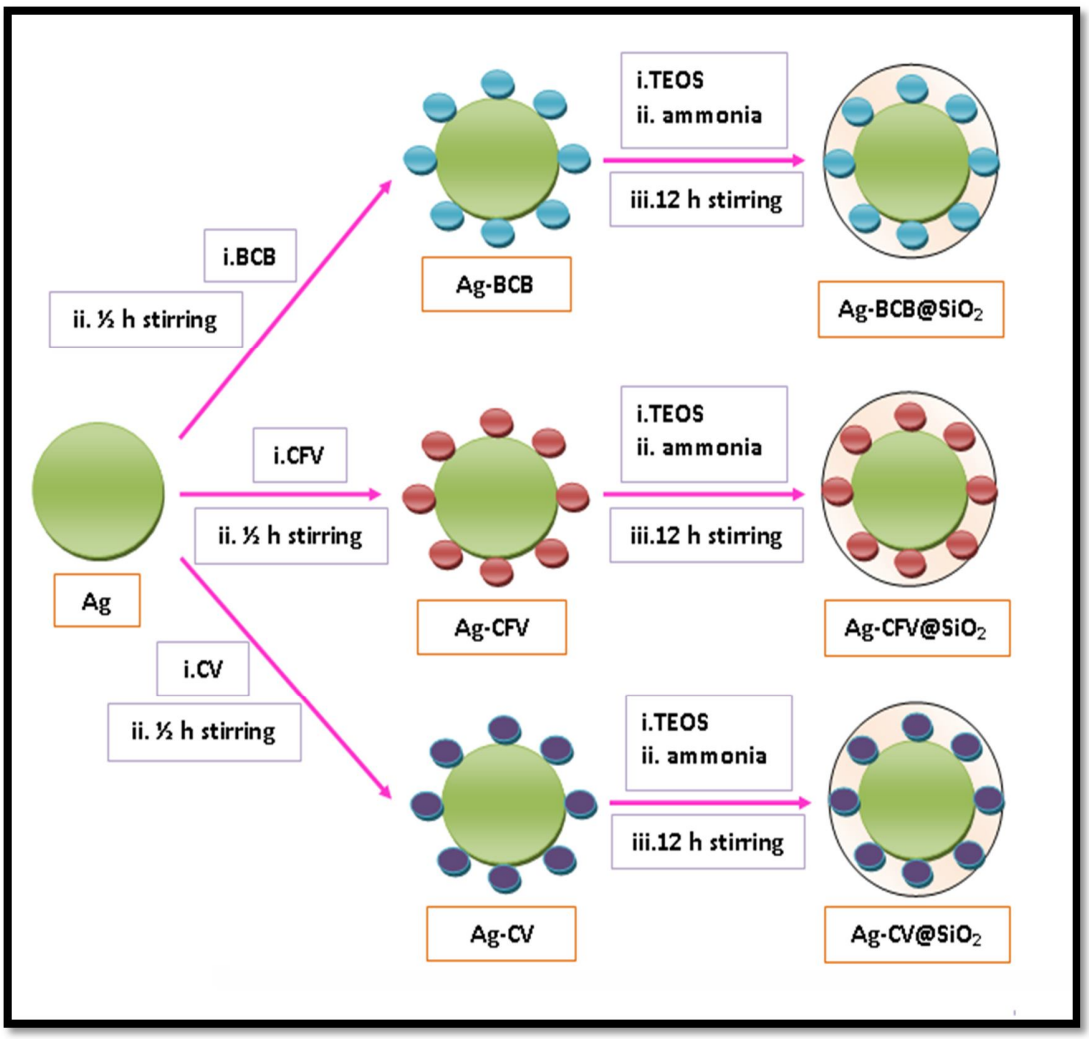

Figure 2.9 Preparation of SERS nanotags, Ag-BCB@SiO_2, Ag-CFV@SiO_2, and Ag-CV@SiO_2 with embedding method for $[dye]_{rxn}$ is 10^{-3} M and [TEOS]/[water] is $9x10^{-5}$.

2.3.5 Preparation of Dual-Dye Doped SERS Nanotags, Ag-BCB-CFV@SiO_2 for Multiplex Analysis

Dual-dye doped nanotags were prepared according to the embedding method applied for single-dye doped nanotags. To ethanol-water solution involving Ag colloids,

solutions of BCB and CFV were added to adjust the molar ratio as BCB:CFV= 1:1, 1:0.8, 1:0.6 and 1:0.4 (Figure 2.10), at constant [BCB] of 10^{-3} M. After 30 min for conjugation, TEOS ([TEOS]/[water]=$9x10^{-5}$) and ammonia were added consecutively. The reaction proceeded for 12 hours under stirring.

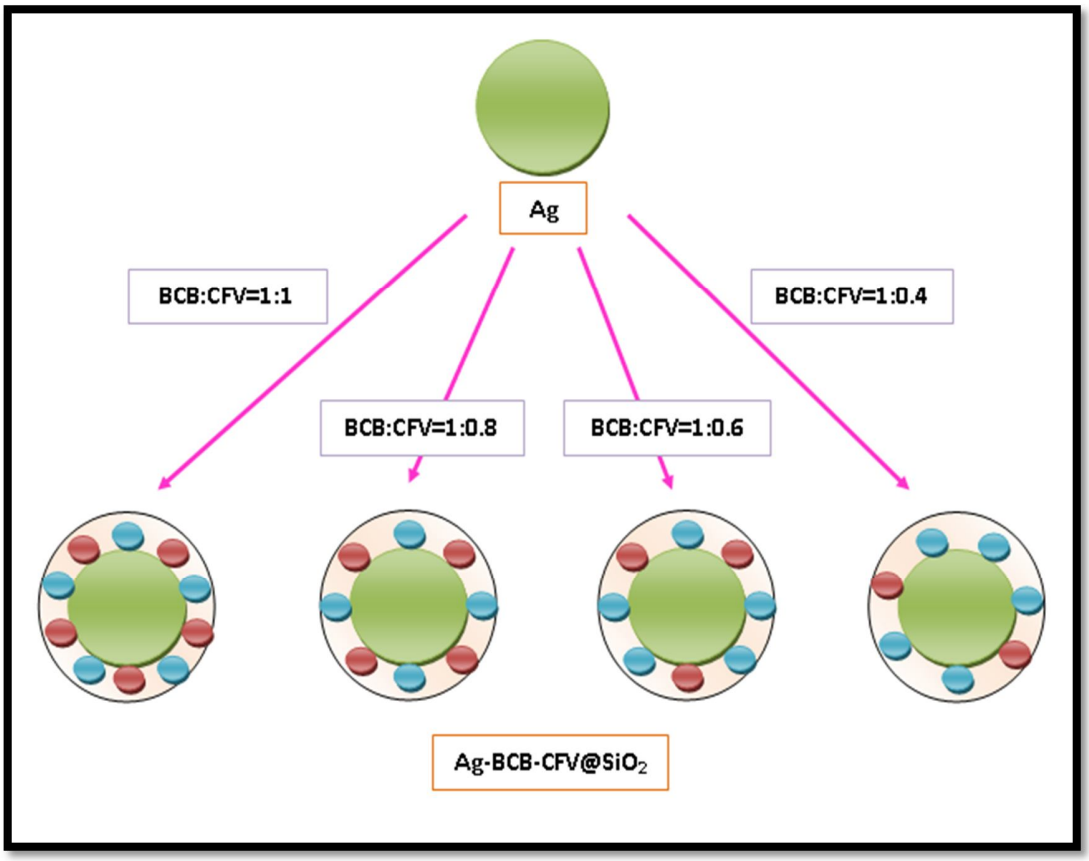

Figure 2.10 Preparation of dual-dye doped SERS nanotags, Ag-BCB-CFV@SiO_2 with embedding method by varying [BCB]/[CFV] as 1:1, 1:0.8, 1:0.6, and 1:0.4.

CHAPTER 3

RESULTS AND DISCUSSION

In the recent study, different single dye-doped and multiple dye-doped SERS nanotags based on Ag nanoparticles were prepared aiming multiple analysis. A typical nanotag was formed by first placing a Raman reporter on the surface of Ag-nanoparticle, thereby creating a known SERS spectrum of that molecule. Then, the label molecule-metal particle is encapsulated in a protective silica shell to eliminate the influence of environmental conditions on the Raman signal. Thus, in our studies, the term SERS nanotag refers to this final structure, Ag-Raman reporter@silica.

In our studies a multiplexing approach was followed, where many distinct SERS nanotags were prepared by using only three Raman label molecules namely BCB, CFV and CV:

i. Three single dye-doped SERS nanotags, Ag-BCB@SiO_2, Ag-CFV@SiO_2, Ag-CV@SiO_2 were prepared by using either BCB, CFV or CV alone.

ii. Four multiple dye-doped SERS nanotags, Ag-BCB-CFV@SiO_2 were prepared by utilizing binary combinations of BCB and CFV in different molar ratios (BCB:CFV=1:1, 1:0.8, 1:0.6 and 1:0.4).

This section has been divided into four subsections. In the first one, it was discussed the formation of Ag nanoparticles using citrate reduction method. Secondly, the deposition of uniform silica shells with tailored thickness using modified Stöber process was described. Thirdly, this silica coating procedure was applied to form SERS nanotag, Ag-BCB@SiO_2. Finally, the last section is devoted to the preparation of different single-dye and dual-dye doped SERS nanotags. For characterizaton studies, Field Emission-Scanning Electron Microscopy (FE-SEM) was used. Optical properties and SERS activity were investigated with UV–visible spectroscopy and Raman spectroscopy, respectively.

3.1 Synthesis of Ag Particles

In our research group, citrate reduction method had already been optimized for the preparation of Ag nanoparticles. Here, these optimized conditions were followed during the synthesis of Ag core nanoparticles.

The resulting Ag particles exhibited spherical shape with a small portion of nanorods as seen in FE-SEM image shown in Figure 3.1. Calculations have shown that the synthesized nanospheres were uniform with a particle size of 64±16 nm.

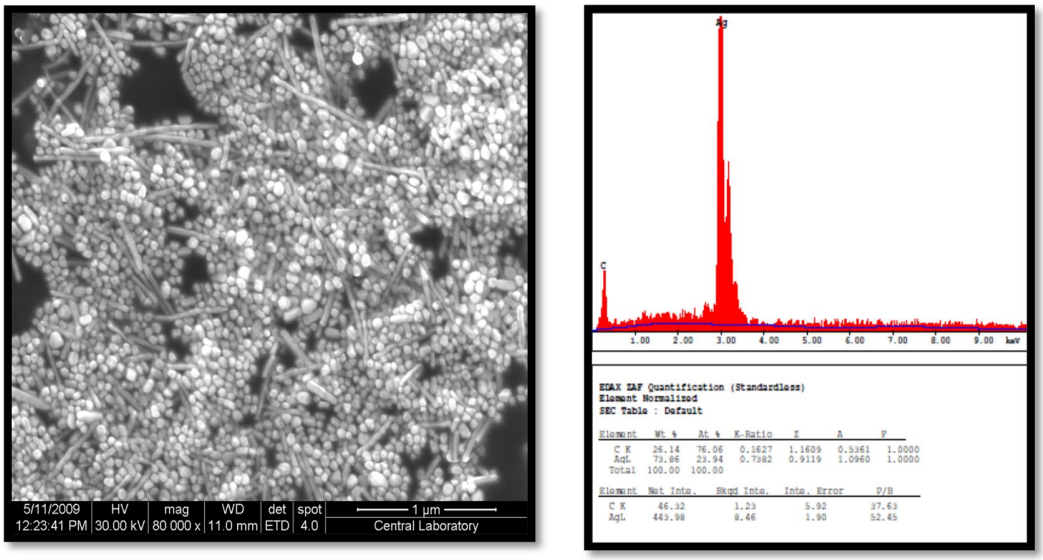

Figure 3.1 FE-SEM image (left) and EDX image (right) of Ag colloids prepared using citrate reduction method.

As well as SEM, UV-vis measurement has also great importance for the characterization and the discussion of the optical properties of the prepared nanoparticles. Ag nanoparticles produce a plasmon resonance peak at 420 nm. In addition, any red shift of the absorption band in a medium of constant dielectric properties points out an increase in the particle size [141]. Besides, silver particles aggregation can be inspected by the existence of surface plasmon resonance coupling band of silver nanoparticles which appears as a weak peak at around 700 nm [142]. The plasmon band of prepared Ag nanoparticles is shown in Figure 3.2. A high intensity, narrow band width plasma resonance peak at 420 nm seen at the related spectrum indicates the formation of Ag nanoparticles with high absorptivity localized surface plasmons. Moreover, the absence of an additional peak around 700 nm proves that there is no aggregation of particles.

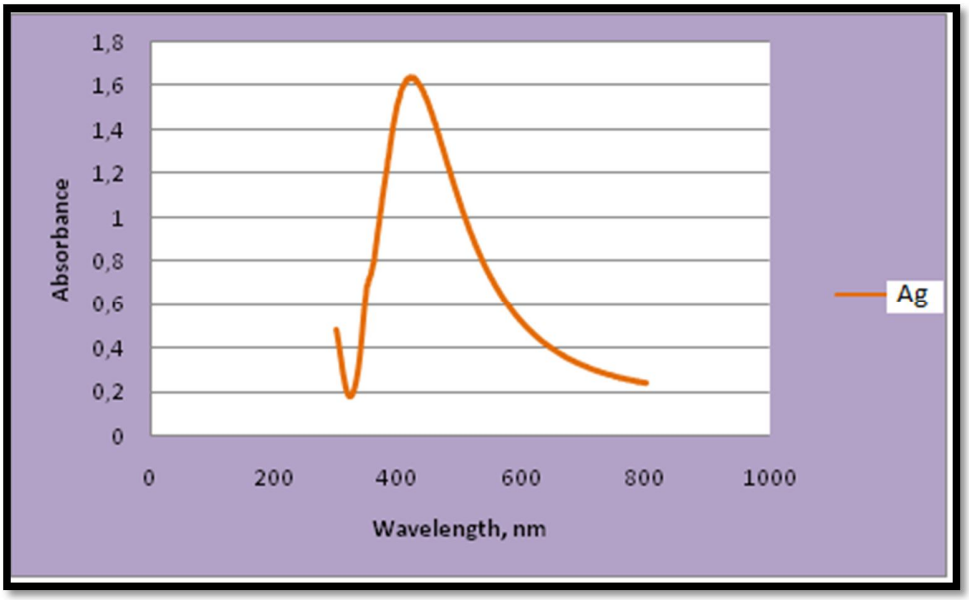

Figure 3.2 Absorption spectrum of Ag colloids prepared using citrate reduction method.

3.2 Preparation of Ag@SiO_2 Particles

3.2.1 Deposition Technique

Two different methods were investigated for efficiency on the formation of an appropriate silica coating and colloidal stability. Both Procedure A and Procedure B are basically modified forms of Stöber method [126]. In Procedure A, co-solvent was ethanol and reaction time was 12 hour at room temperature whereas isopropanol was cosolvent and the reaction requires 30 min at room temperature and additional 20 hours at 4^0C in Procedure B. For both, [TEOS]/[water] and amount of ammonia to be added were kept constant at $2x10^{-4}$ and 6.7 ml, respectively. Surface morpologies of Ag@SiO_2 composites prepared were examined by FE-SEM images recorded and depicted in Figure 3.3.

a.

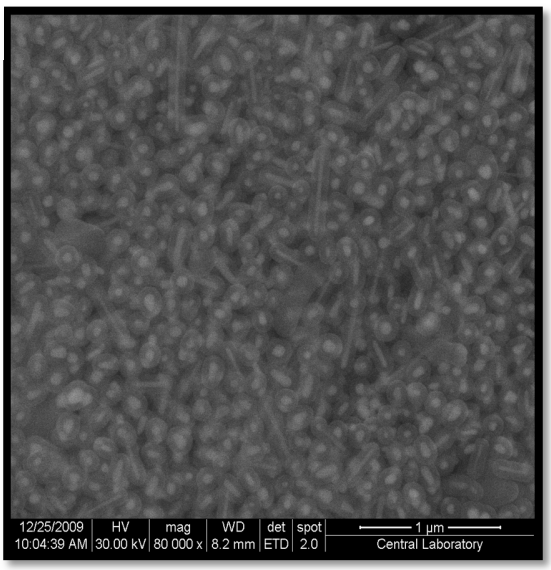

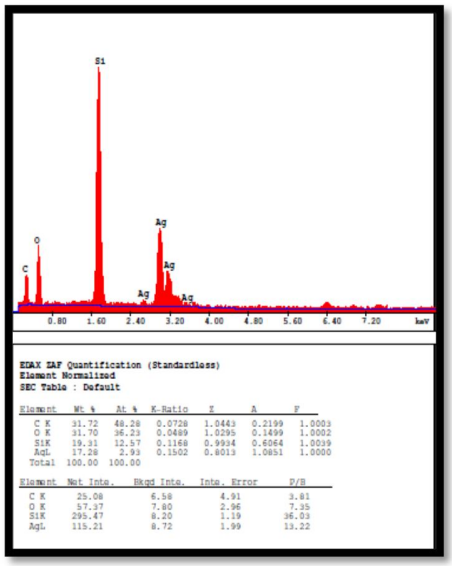

b.

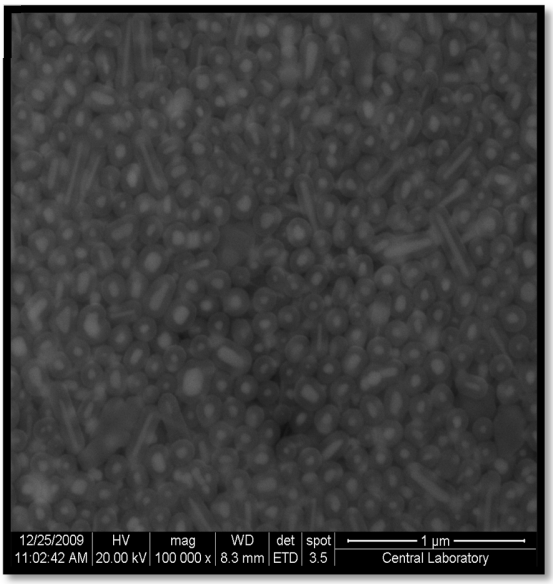

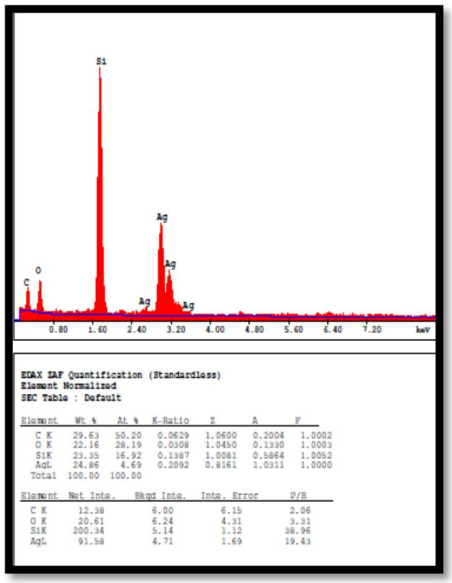

Figure 3.3 Fe-SEM images (left) and EDX images (rigth) of Ag@SiO_2 composites prepared using two deposition methods, a.Procedure A, and b.Procedure B.

In Figure 3.3, brighter center part is corresponding to silver and silica layer appears pale. In both procedures, it was observed a homogeneous silica shell around particles. The calculated mean values for silica thickness were 49±3 nm for Procedure A and 40±3 nm for Procedure B. The absorption spectra of Ag@SiO_2 composites prepared using Procedure A and Procedure B are given in Figure 3.4.

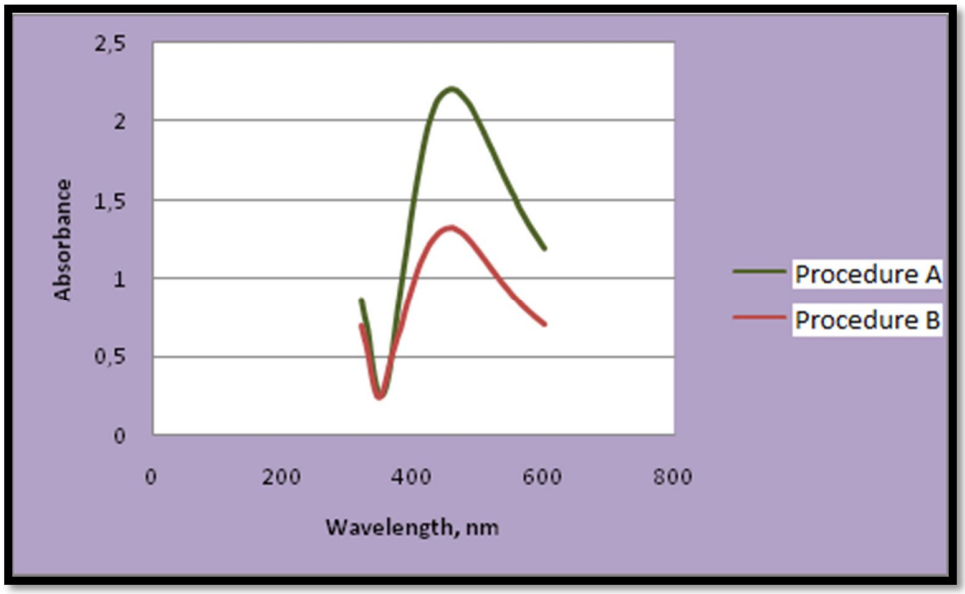

Figure 3.4 Absorption spectra of Ag@SiO_2 composites prepared using two deposition methods, Procedure A and Procedure B.

As seen in Figure 3.4, resulting Ag@SiO_2 composites in both procedures has surface plasmon peak location at 460 nm for both procedures. Although particles prepared by both procedures provided plasmon resonance peak of Ag, the intensity of one prepared by Procedure B was weaker than that by Procedure A. This decrease was actually due to the partial aggregation of the particles observed. On the other hand,

aggregate formation was not observed in Procedure A. It was decided that Procedure A will be followed during further examinations.

3.2.2 Effect of [TEOS]/[Water] on Silica Thickness

The precise control of the thickness of the shell is very important in the nanotag preparation. The common approach to vary shell thickness is to control the molar ratio of the sol-gel precursor, TEOS to water. Here, [TEOS]/[water] was varied in a range of $6x10^{-4}$-$7x10^{-5}$ at constant reaction conditions. The change in the cell thickness was monitored by FE-SEM measurements and the related images are shown in Figure 3.5.

a.

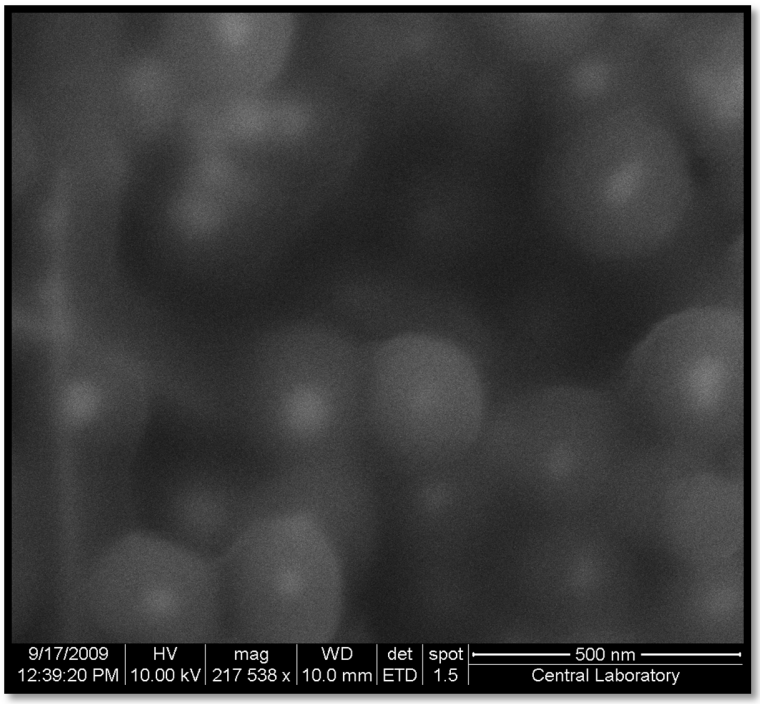

b.

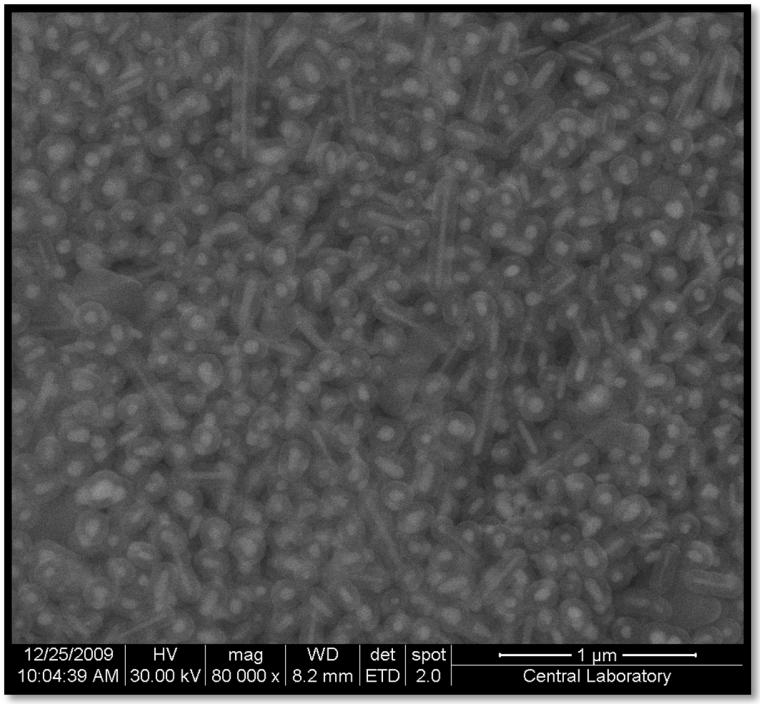
12/25/2009 | HV | mag | WD | det | spot | 1 µm
10:04:39 AM | 30.00 kV | 80 000 x | 8.2 mm | ETD | 2.0 | Central Laboratory

c.

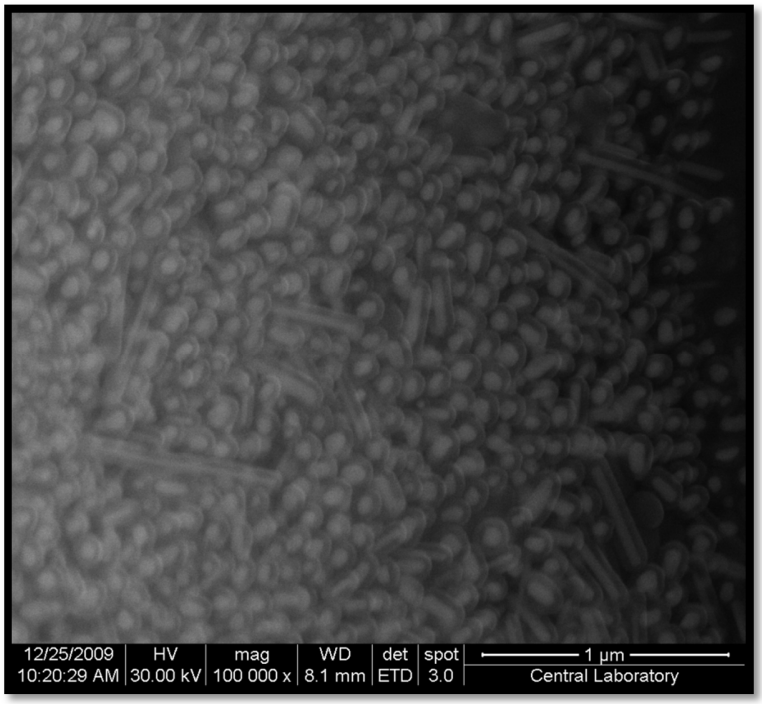
12/25/2009 | HV | mag | WD | det | spot | 1 µm
10:20:29 AM | 30.00 kV | 100 000 x | 8.1 mm | ETD | 3.0 | Central Laboratory

d.

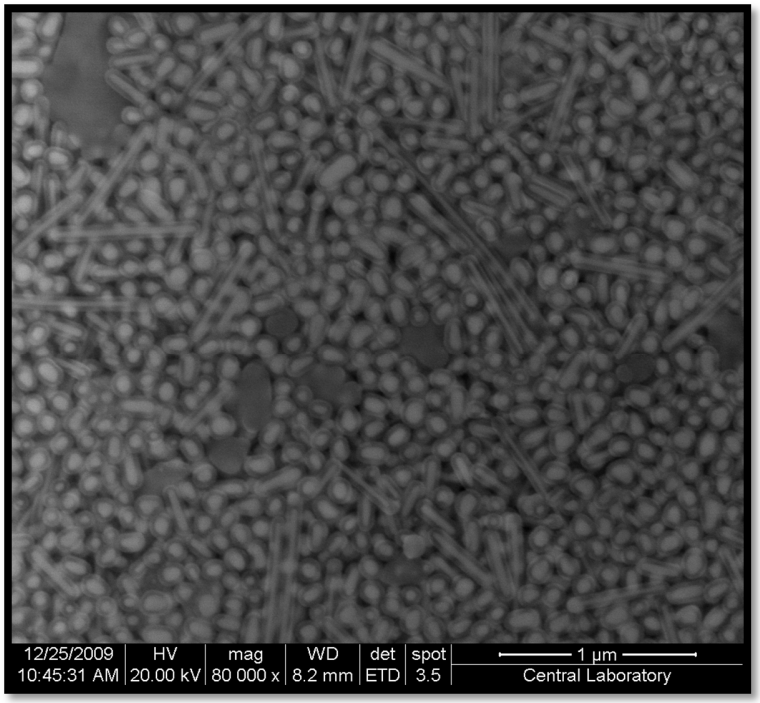
12/25/2009 | HV | mag | WD | det | spot | 1 µm
10:45:31 AM | 20.00 kV | 80 000 x | 8.2 mm | ETD | 3.5 | Central Laboratory

e.

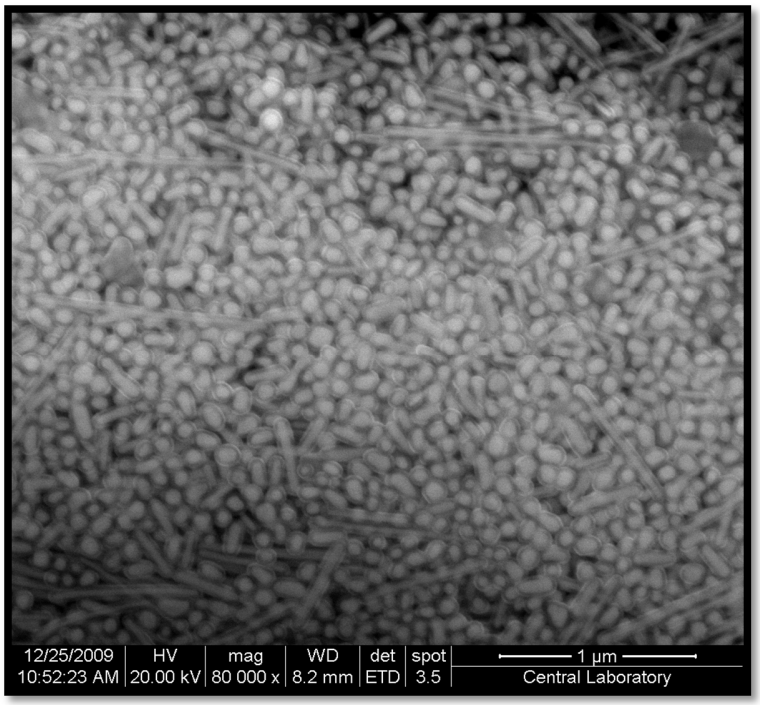
12/25/2009 | HV | mag | WD | det | spot | 1 µm
10:52:23 AM | 20.00 kV | 80 000 x | 8.2 mm | ETD | 3.5 | Central Laboratory

f.

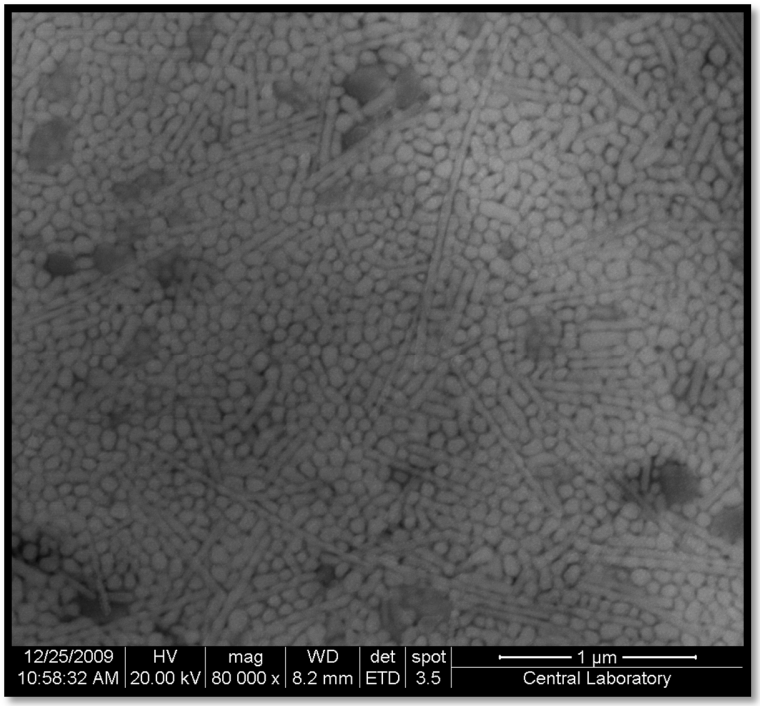

Figure 3.5 FE-SEM images of resulting Ag particles prepared using Procedure A by varying [TEOS]/[water] as a. $6x10^{-5}$, b. $2x10^{-4}$, c. $1x10^{-4}$, d. $9x10^{-5}$, e. $8x10^{-5}$, and f. $7x10^{-5}$.

As seen in Figure 3.5, the decrease in the [TEOS]/[water] leads to a decrease in the silica shell thickness. However, for the ratio $7x10^{-5}$, there was no silica deposition around the Ag particles. Hence, it was concluded that silica coating at desirable thicknesses can be achieved by only adjusting the TEOS concentration at the investigated [TEOS]/[water] and the decrease in the concentration of TEOS down to a defined value cause silica coating not to be formed. The variation of thickness with [TEOS]/[water] is summarized in Table 3.1.

Table 3.1 Silica thickness of $Ag@SiO_2$ particles prepared by varying [TEOS]/[water] in Procedure A.

[TEOS]/[water]	$6x10^{-4}$	$2x10^{-4}$	$1x10^{-4}$	$9x10^{-5}$	$8x10^{-5}$	$7x10^{-5}$
Thickness, nm	179±20	49±3	36±2	26±3	22±2	---

The extent of the red shift in the nominal wavelength of the localized surface plasmon absorption peak due to the increased shell thickness was followed with UV-vis absorption measurements and the related spectra is shown in Figure 3.6 and the localized surface plasmon absorption positions of $Ag@SiO_2$ particles at the specified silica shell thickness are summarized in Table 3.2.

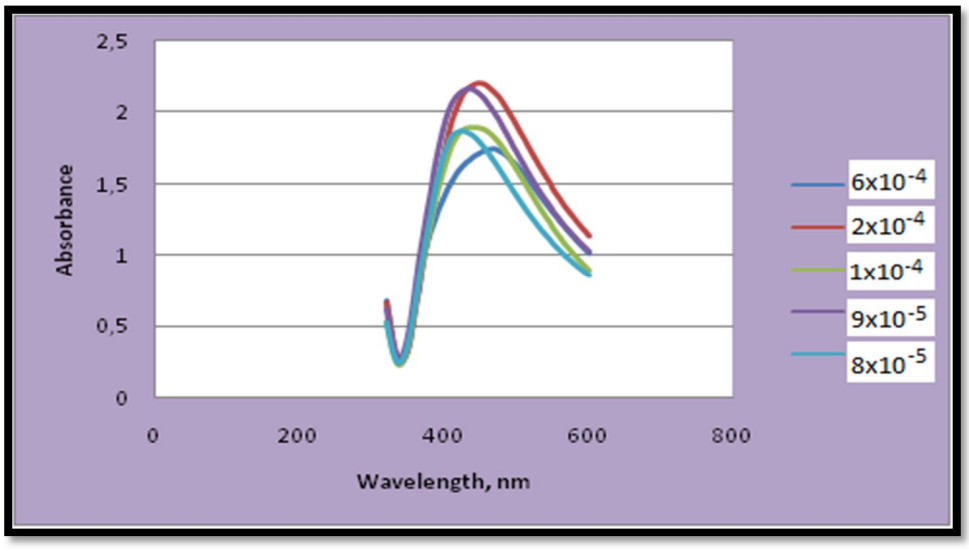

Figure 3.6 Absorption spectra of $Ag@SiO_2$ particles prepared by varying [TEOS]/[water] from $6x10^{-4}$ to $8x10^{-5}$ in Procedure A.

Table 3.2 Plasmon absorption peak locations of $Ag@SiO_2$ particles having various silica thickness.

Thickness, nm	179±20	49±3	36±2	26±3	22±2
λ_{max}, nm	475	460	450	435	425

As indicated in Table 3.2, an obvious red shift was observed following silica coating considering that localized surface plasmon of bare Ag particles has an absorption peak centered at 420 nm (Figure 3.1). This is an expected behavior because the location of resonance plasmon band is highly dependent on the properties of medium for same sized-particles. Thus, when Ag particles were coated with silica, the local refractive index of surrounding medium was increased and relatedly, the surface plasmon absorption band experienced a red shift [143].

3.2.3 SERS Enhancement by Ag and $Ag@SiO_2$ Particles

Silver nanoparticles produce strong electric field with the help of their localized surface plasmons. On this basis, examination of the SERS enhancement property of the silver nanoparticles prepared and the effect of silica coating on the enhancement carry a crucial importance. They should enhance the signal but do not give any background signal. Therefore, Raman spectra of glass slide used in measurements, Ag colloids and $AgSiO_2$ particles alone were measured, as shown in Figure 3.7, at an acquisition time of 10 s (10 times longer than the acquisition time normally used in this study).

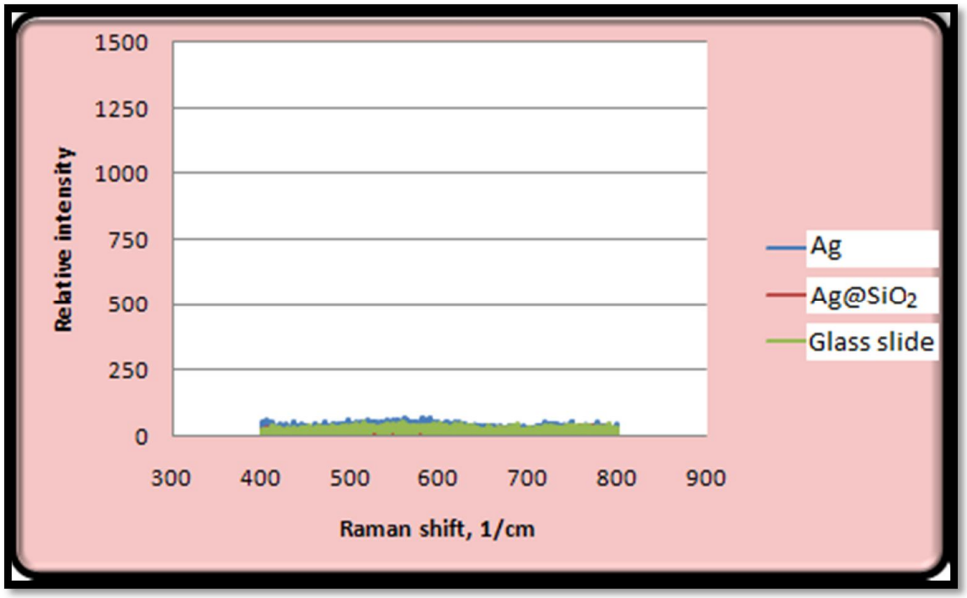

Figure 3.7 Raman spectra of the glass slide, Ag colloids, and Ag@SiO_2 particles.

As seen in related Raman spectra (Figure 3.7), none of them yield any Raman signal. Hence, they all are not Raman scatterer, as expected. To evaluate the enhancement provided by Ag colloids and to see whether there is any effect of silica deposition on this enhancement, first Raman signal of 10^{-6} M BCB solution was acquired on a glass slide and then the Raman spectra of 10^{-8} M BCB solution was measured both by utilizing Ag colloids and Ag@SiO_2 composites as substrates. The spectra are presented in Figure 3.8.

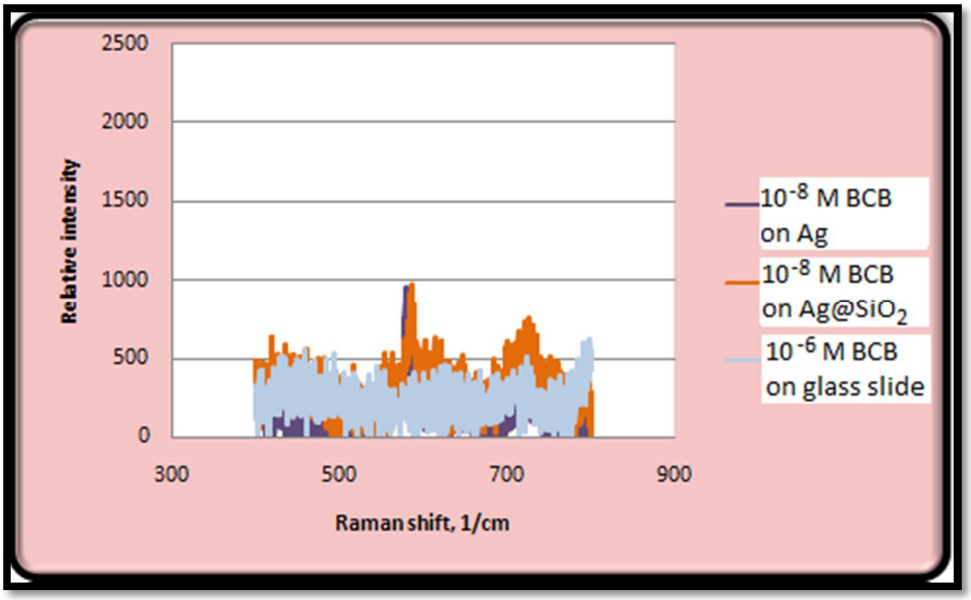

Figure 3.8 Raman spectra of 10^{-6} M BCB on the glass slide and 10^{-8} M BCB on Ag and $Ag@SiO_2$ particles as substrate.

As can be seen in Figure 3.8, the signal of 10^{-6} M solution of BCB could not be obtained with normal Raman measurement whereas SERS spectra of even 10^{-8} M solution of BCB were acquired successfully when Ag colloids were used as a substrate at the same acquisition time (10 s). In addition, when we looked at spectrum of 10^{-8} M solution of BCB measured on $Ag@SiO_2$ composites, any significant change in signal intensity was not observed. It was concluded that thus prepared silver nanoparticles could magnify the Raman signals significantly and silica deposition does not lead any decrease in the enhancement provided by Ag particles and both can be used in any type of SERS measurements.

3.3 Preparation of A Single-Dye Doped SERS Nanotag, Ag-BCB@SiO_2

A SERS nanotag, here, is the silica coated dye conjugated Ag particles. BCB is a positively charged dye, having high Raman intensity and used as Raman reporter dye in this study. The structure of BCB (inset) and the Raman spectrum [79] is presented in Figure 3.9. The characteristic peak of BCB seen in Figure 3.9 corresponds to the benzene ring deformation mode [144].

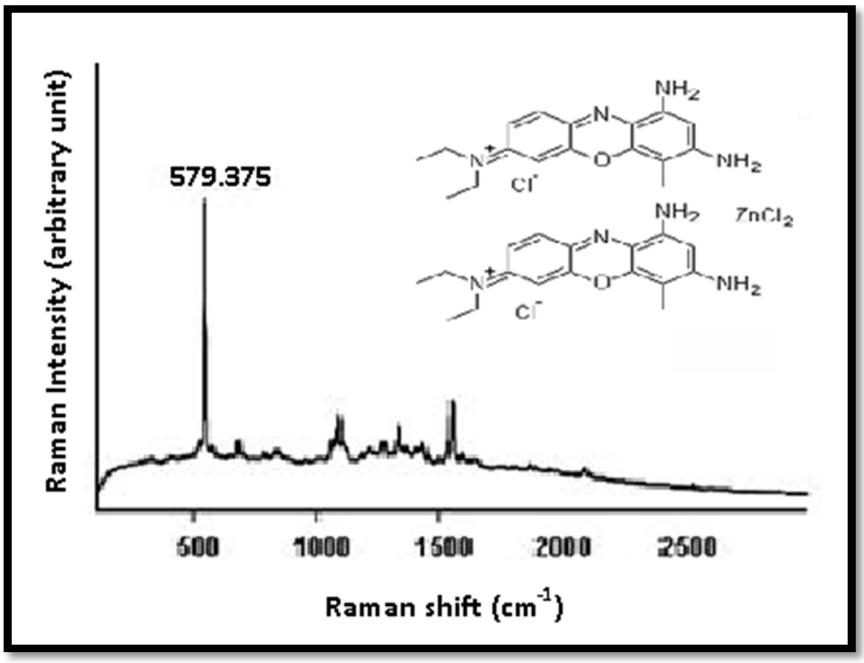

Figure 3.9 Structure and Raman spectrum of BCB [79].

For encapsulation dye in the nanotag structure, first, two methods were examined and then, effect of thickness and dye concentration on the resulting signal intensity were investigated.

3.3.1 Encapsulation Method

Here, the effectiveness of two different methods was tested for encapsulate dye molecules into the silica network, namely impregnation and embedding. Impregnation method considers the penetration of dye in the depth of the silica coating when Ag@SiO_2 particles were submerged in the alcoholic solution of Raman reporter dye. On the other hand, in the embedding method, dye molecules are first conjugated to Ag particles and the silica deposits on these dye conjugated-Ag particles. Concentration of BCB and [TEOS]/[water] were kept constant in both methods at 10^{-4} M and $9x10^{-5}$, respectively. The FE-SEM images of Ag-BCB@SiO_2 nanotags prepared via both impregnation and embedding methods are given in Figure 3.10.

a.

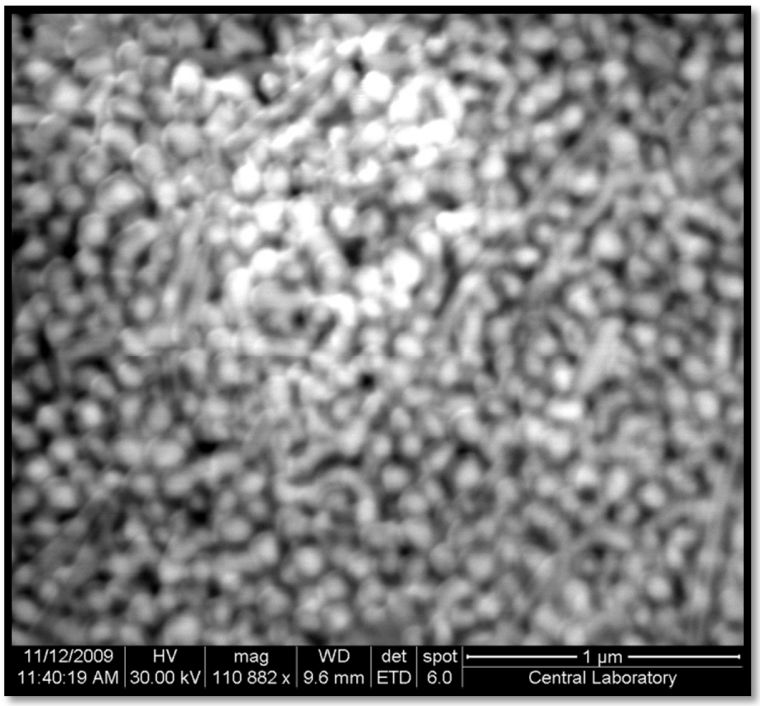

b.

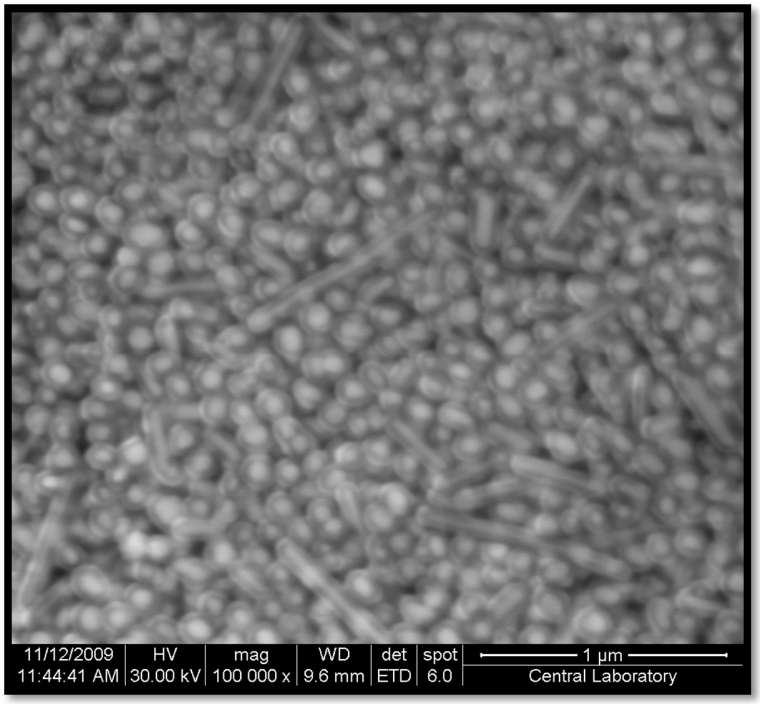

Figure 3.10 FE-SEM images of Ag-BCB@SiO_2 nanotags prepared by two encapsulation methods, a. impregnation, and b. embedding.

The silica layer thicknesses for Ag-BCB@SiO_2 nanotags resulting from impregnation method (Figure 3.10.a) and embedding method (Figure 3.10.b) were calculated and found out as 30±2 and 35±3 nm, respectively. Considering that thickness is 26±3 nm for Ag@SiO_2 for [TEOS]/[water]=9x10^{-5} (Section 3.2.2), results have shown that impregnation method did not cause any significant increase in the shell thickness. However, a thicker silica shell formation was observed for the particles synthesized via embedding method.

The SERS properties of these Ag-BCB@SiO_2 nanotags prepared by means of two encapsulation methods were investigated using Raman spectroscopy at the

wavenumber region of the BCB scattering and the related spectra is presented in Figure 3.11.

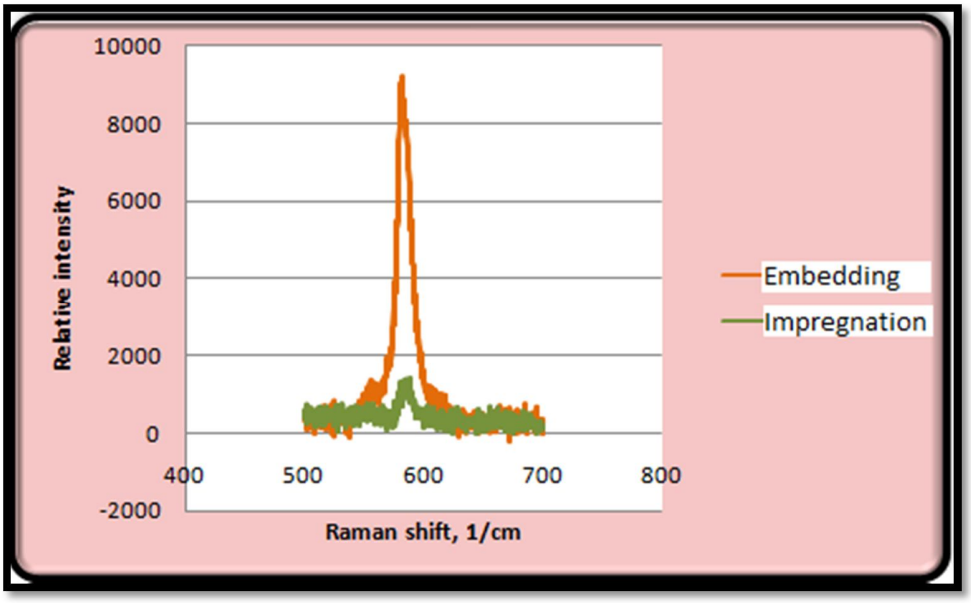

Figure 3.11 Raman spectra of Ag-BCB@SiO_2 nanotags prepared by two encapsulation methods, impregnation and embedding.

As seen in Figure 3.11, Raman nanotags prepared by embedding method gave much more intense peak for BCB compared to the one prepared with impregnation method. This decline in the signal could be explained by the alteration of BCB concentration due to the dye leakage and/or incomplete penetration. Diffusion of the dye into the silica is essential for the preparation of the nanotag through impregnation method. Penetration at the external surface of the Ag@SiO_2 particles could be easy. However, the penetration of dye in the depth direction to the silver surface is clearly more difficult. Besides, just as the dye can enter the gel, it can also leach from the gel.

Leaching limits their applications especially in biologically relevant fields. Therefore, embedding method was chosen as the encapsulation method.

3.3.2 Effect of Various Silica Thickness on Encapsulation

It is desirable to have dense packing of Raman reporters for maximum brightness. Tunability of the silica shell thickness by controlling the molar ratio of TEOS to water, [TEOS]/[water] was mentioned formerly in Section 3.2.2. In this part, the influence of the silica thickness on the SERS intensity of BCB was discussed. For constant concentration of BCB at 10^{-4} M, [TEOS]/[water] was varied exclusively in the preparation of the nanotags. The spectral evolution of the BCB signal of nanotags for different [TEOS]/[water] and so different silica thicknesses is shown in Figure 3.12.

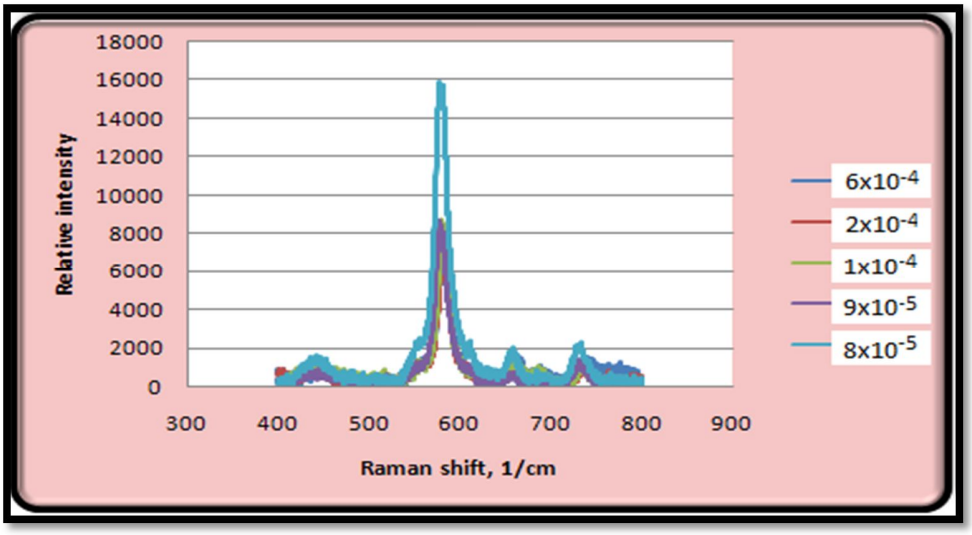

Figure 3.12 Raman spectra of Ag-BCB@SiO_2 nanotags prepared by varying [TEOS]/[water] from $6x10^{-4}$ to $8x10^{-5}$ in the embedding method.

As seen in Figure 3.12, the highest signal intensity was obtained when [TEOS]/[water] was $8x10^{-5}$, corresponding to the lowest TEOS concentration and the thinnest silica thickness 22±2 nm for Ag@SiO_2. At higher and smaller ratios, the relative Raman intensities of the nanotags were in the range of all 6000-8000, far from 16000. This high intensity was the goal that we would like achieve. Afterwards the stability of the particles having the [TEOS]/[water] ratio of $8x10^{-5}$ and $9x10^{-5}$ in water were examined. For this purpose Ag-BCB@SiO_2 nanotag samples of ratios $8x10^{-5}$ and $9x10^{-5}$ were redispersed in water and stored for 1 week. The Raman spectra of the nanotag particles collected through centrifugation were measured and are depicted in Figure 3.13 and Figure 3.14.

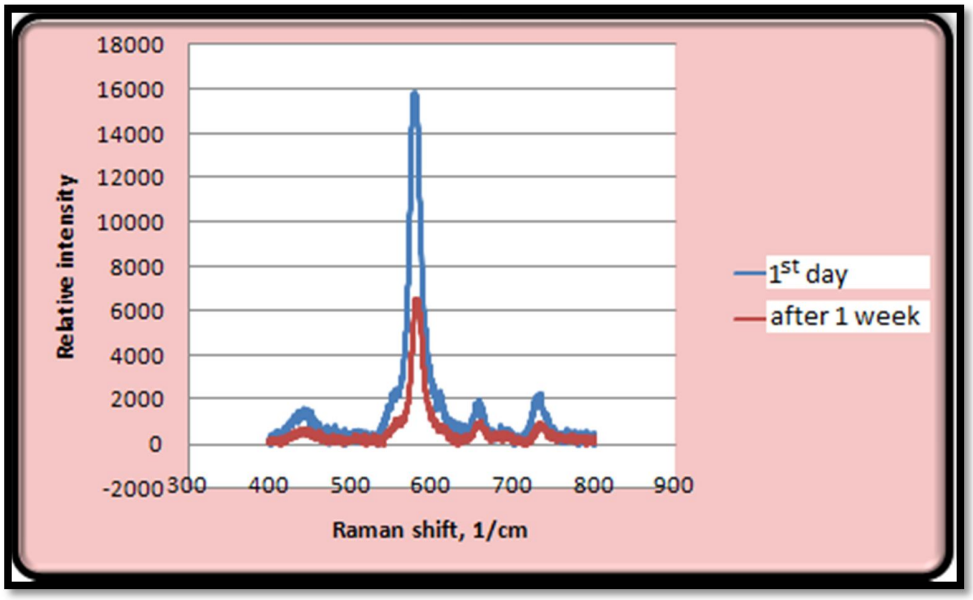

Figure 3.13 Raman stability of Ag-BCB@SiO_2 nanotag prepared using [TEOS]/[water] as $8x10^{-5}$ in the embedding method.

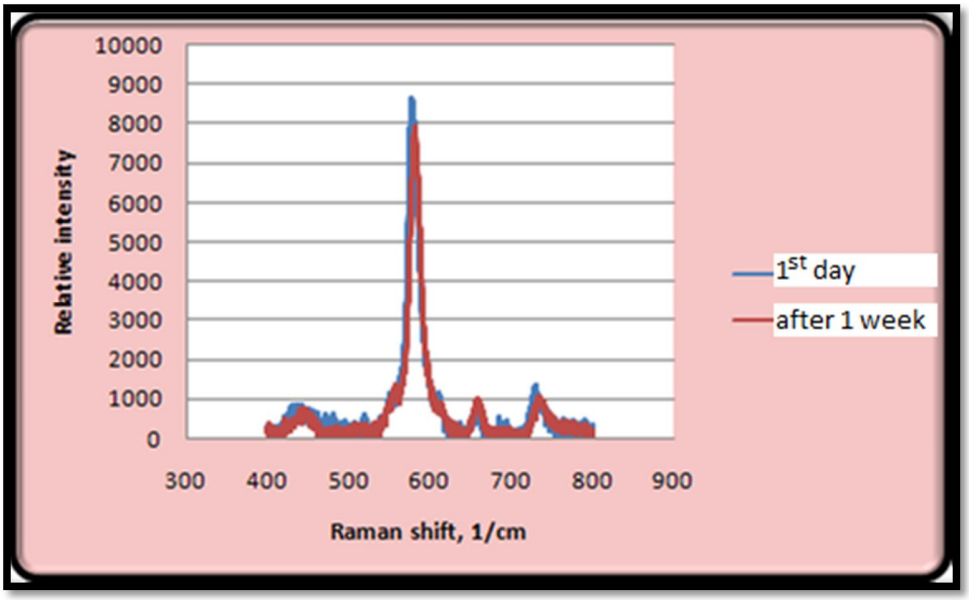

Figure 3.14 Raman stability of Ag-BCB@SiO_2 nanotag prepared using [TEOS]/[water] as $9x10^{-5}$ in the embedding method.

The signal intensity of the Ag-BCB@SiO_2 particles prepared at the [TEOS]/ [water] of $8x10^{-5}$ was diminished % 58 (Figure 3.13) whereas that of the nanotags prepared at the [TEOS]/ [water] of $9x10^{-5}$ was decreased only 2.0 % (Figure 3.14). Hence, it was concluded that, in order to prevent the leaching of the dye, the structure of the silica was critical and at low concentration of TEOS, the required impenetrable silica matrix could not be achieved. In other words, the stability of the particles prepared at a ratio of $8x10^{-5}$ was worse than that of the particles prepared at a ratio of $9x10^{-5}$. Therefore although the signal intensity of the latter was low, due to its stability, [TEOS]/ [water] of $9x10^{-5}$ was adopted for silica coating. Once the preparation of the nanotags was optimized, than the signal reproducibility of the nanotags produced at different batches was investigated. For this purpose five replicates of Ag-BCB@SiO_2 nanotags were prepared at the optimized conditions and batch to batch variations in the Raman signal of the nanotags prepared were examined. The variation in terms of RSD was

found as 3.8 %. Therefore, it was concluded that thus prepared Ag-BCB@SiO_2 nanotags were very stable and reproducible.

3.3.3 Effect of Total Dye Concentration on Encapsulation

In the previous sections related to the nanotag studies, the concentration of BCB in the reaction medium was 10^{-4} M. Here, lower and higher BCB concentration was examined for the effect of dye concentration in the medium on the resulting signal intensity. The Raman spectra of the Ag-BCB@SiO_2 nanotags prepared using different concentrations of BCB are depicted in Figure 3.15.

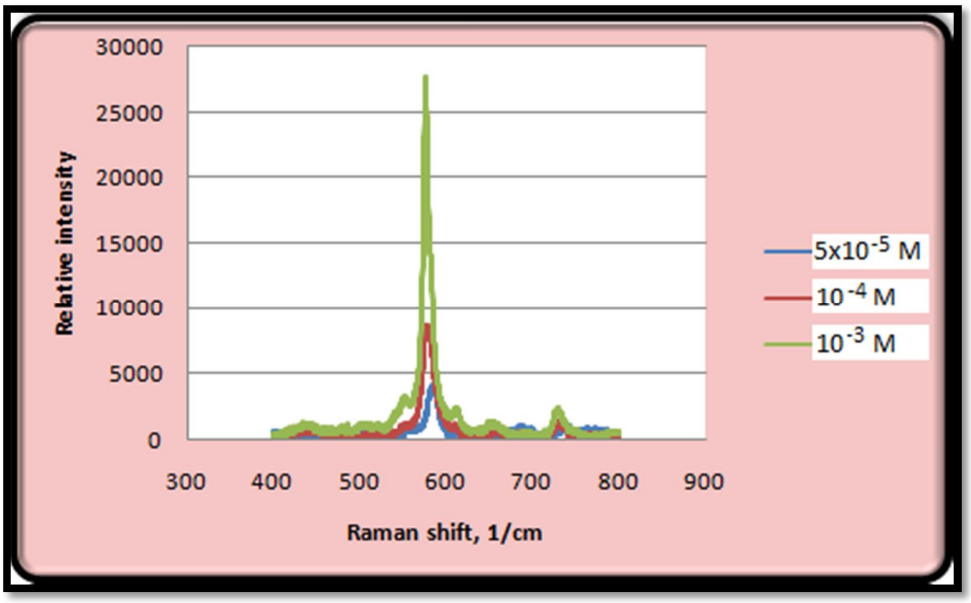

Figure 3.15 Raman spectra of Ag-BCB@SiO_2 nanotags prepared by varying $[BCB]_{rxn}$ from $5x10^{-5}$ to 10^{-3} M in the embedding method.

As can be seen in Figure 3.15, the relative intensity of the SERS signal increases from 4000 to 30000 when the total BCB concentration in the reaction medium was changed from $5x10^{-5}$ M to 10^{-3} M. Taken together, the results presented so far indicated that the Raman intensity of the resulting Ag-BCB@SiO_2, SERS nanotags, prepared using 10^{-3} M [BCB] were intense enough for routine single-nanotag detection even in a complex environments such as a biological medium.

3.4 Preparation of Different Single-Dye Doped SERS Nanotags, Ag-CFV@SiO_2 and Ag-CV@SiO_2 for Multiplex Analysis

As explained before, narrow band width of Raman spectra make SERS nanotags ideal for multiplex analysis for determination of biological compounds. Since the Ag particles are negatively charged, a positively charged dye, BCB was encapsulated and Ag-BCB@SiO_2 SERS nanotags were successfully prepared. In this section, the preparation and the characterization of two more SERS nanotags, Ag-CFV@SiO_2 and Ag-CV@SiO_2 using positively charged Raman active dyes (CFV and CV) were discussed. The structure of CFV (inset) and the related Raman spectrum are depicted in Figure 3.16 [79].

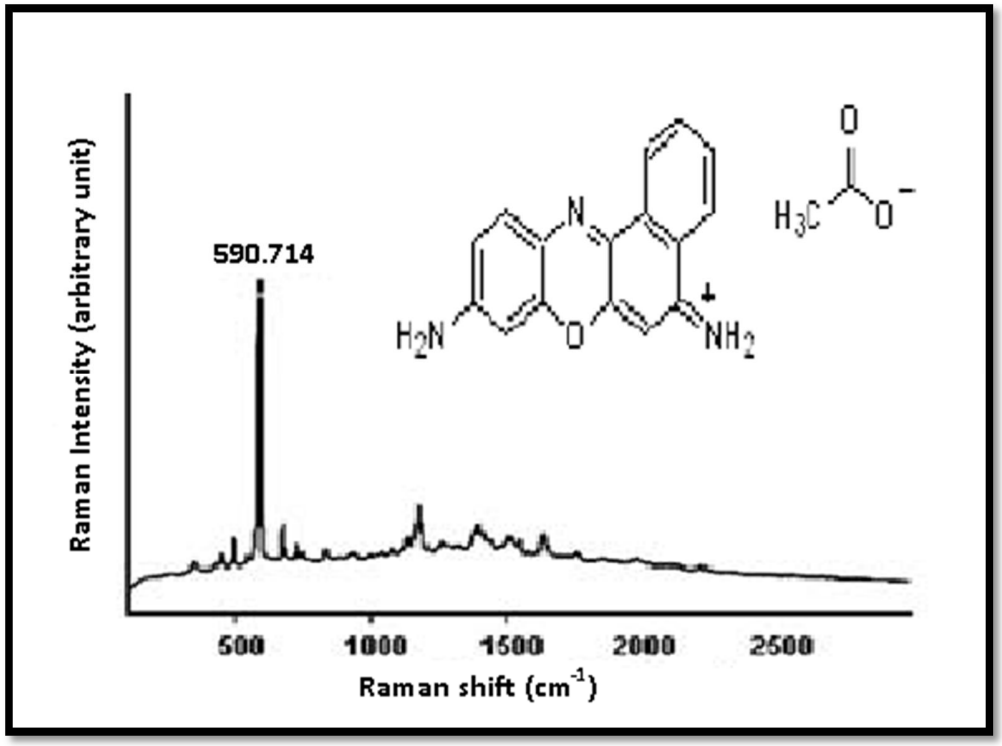

Figure 3.16 Structure and Raman spectrum of CFV [79].

The characteristic peak of CFV seen in Figure 3.16 arises from the benzene ring deformation mode [144]. The structure and the belonging Raman spectrum of CV are given in Figure 3.17 and the characteristic peaks of CV and corresponding bond assignments are summarized in Table 3.3 [145].

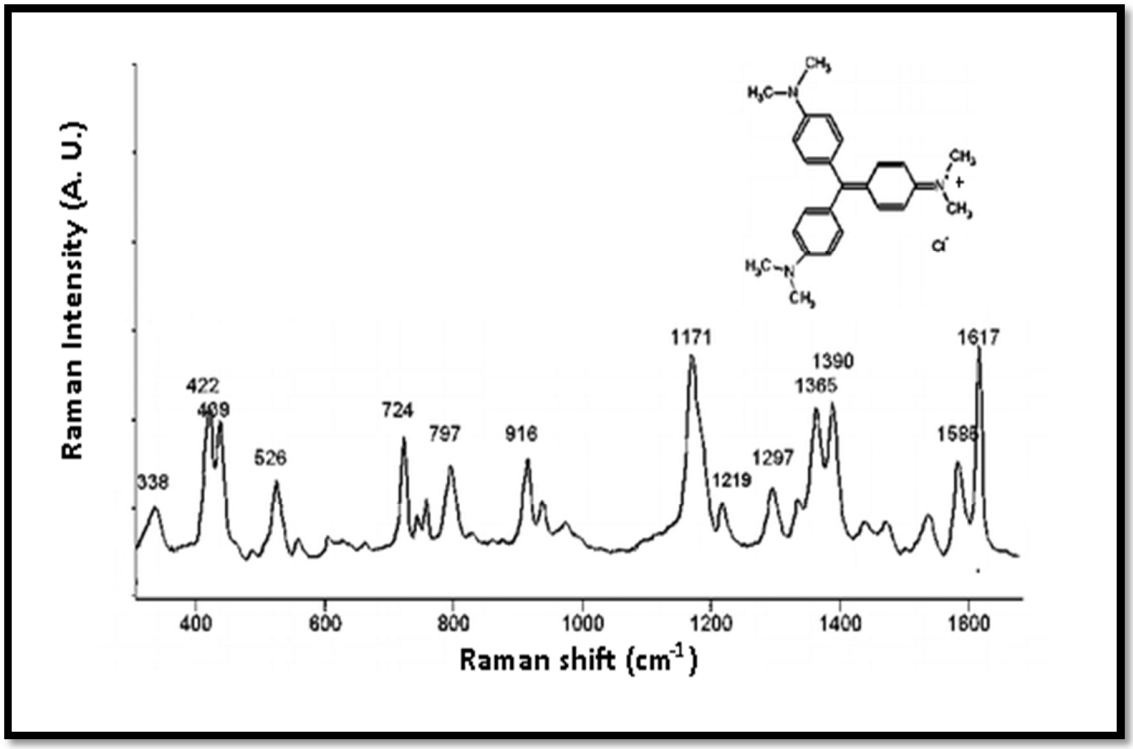

Figure 3.17 Structure and Raman spectrum of CV [144].

Table 3.3 Raman band assignments of CV [144].

Raman shift (cm^{-1})	Band assignment
~338	in-plane vibration of phenyl-C-phenyl
~422	out-of-plane vibrations of phenyl-C-phenyl
~526 and 916	ring skeletal vibration of radical orientation
~724 and 797	out-of-plane vibrations of ring C-H
~1171	in-plane vibrations of ring C-H
~1219	C-H rocking
~1365 and 1390	N-phenyl stretching
~1585 and 1617	ring C-C stretching

The Raman scattering efficiency of BCB and CFV are comparable, on the other hand CV is a weak Raman scatterer. For encapsulation of CFV and CV, the same reaction conditions as optimized in the case of BCB encapsulation were used. Embedding method was performed with a total dye concentration of 10^{-3} M and [TEOS]/[water] of $9x10^{-5}$. SERS spectra of these nanotags, Ag-CV@SiO_2 and Ag-CFV@SiO_2 are given in Figure 3.18 and Figure 3.19, respectively.

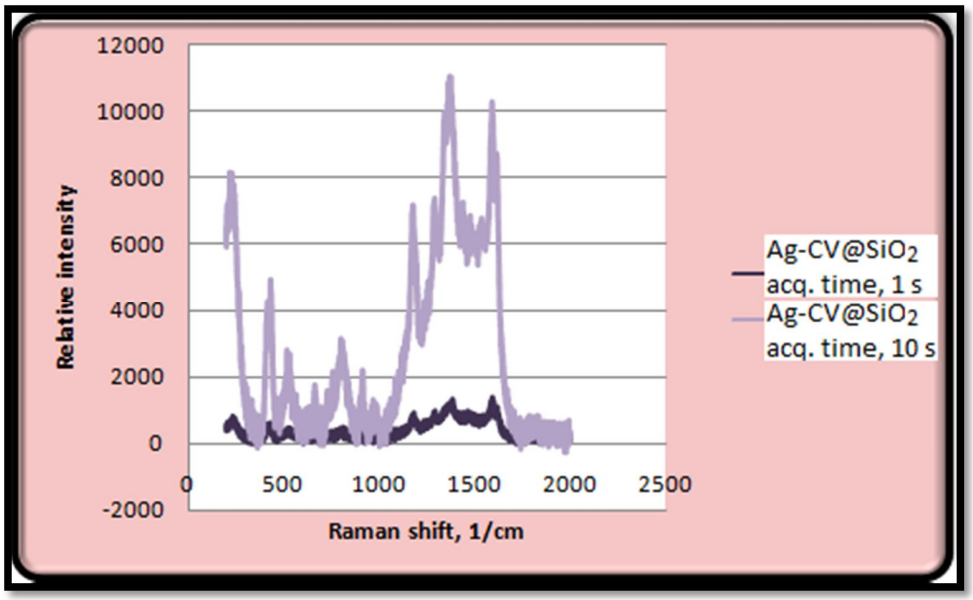

Figure 3.18 Raman spectra of Ag-CV@SiO_2 nanotags, prepared using embedding method for $[CV]_{rxn}$ is 10^{-3} M and [TEOS]/[water] is $9x10^{-4}$, at acquisition time 1s and 10s.

Up to now, through all Raman experiments, the acquisition time has been kept at 1 s. As seen in the Raman spectra of Ag-CV@SiO_2 nanotags (Figure 3.18), it was observed that the nanotag yields weak signal intensity when the acquisition time was 1 s but an intense signal at acquisition time of 10 s.

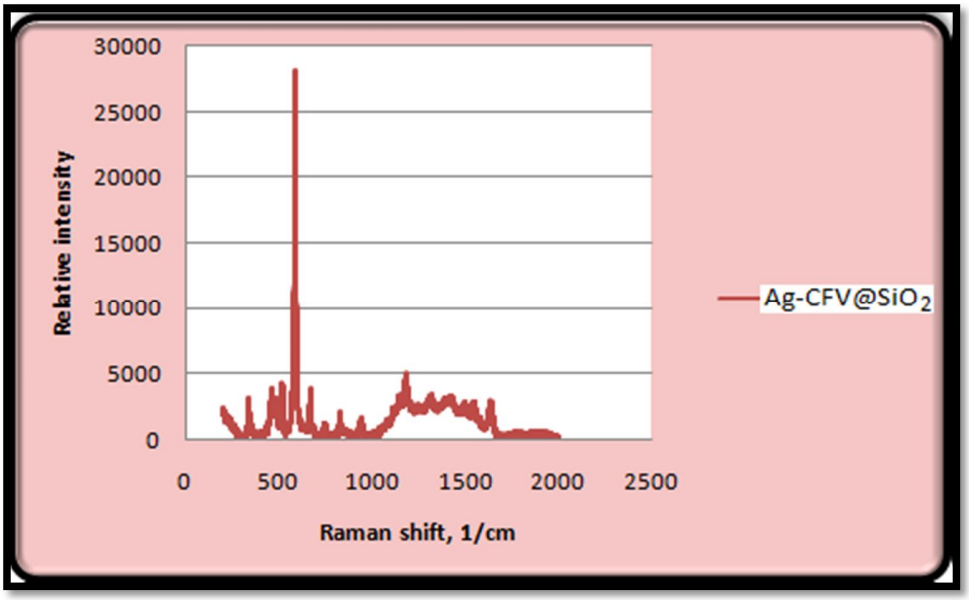

Figure 3.19 Raman spectrum of Ag-CFV@SiO_2 nanotags prepared using embedding method for $[CFV]_{rxn}$ is 10^{-3} M and [TEOS]/[water] is $9x10^{-4}$.

As can be seen in the Raman spectrum (Figure 3.19), Ag-CFV@SiO_2 nanotags yield an intense signal as the characteristics of dye CFV. These studies have shown that, as in the case of BCB, CFV and CV could also be conjugated to Ag particles with electrostatic interactions and encapsulated in the silica core shell structure to form Ag-CFV@SiO_2 and Ag-CV@SiO_2 nanotags with high signal intensity. The use of longer acquisition times would improve the signal intensity further. Although spectral characterizations regarding leaching were not presented here, leakage was not observed for any of the nanotags prepared.

3.5 Preparation of Dual-Dye Doped SERS Nanotags, Ag-BCB-CFV@SiO_2 for Multiplex Analysis

In the nanotag detection systems, considering the great interest and requirement in the development of multiplex analysis, it is a big challenge to design and obtain specific spectral signatures. Synthesis of single-dye doped SERS nanotags can be extended to a large number of individual dyes. Moreover, just doping two dyes at various ratios in the same Ag-SiO_2 nanoparticle can be greatly expand the SERS nanotag-library. Unfortunately, this strategy is limited by the differences in the relative affinity of each dye for the surface [146], and their Raman scattering efficiencies. To accurately control the resultant spectral intensities of the multiplexed signals, the component dyes must have similar spectral behaviors. Raman spectra of the three SERS nanotags prepared are presented in the same graph, Figure 3.20, for a comparison of their signal intensities acquired at the same conditions.

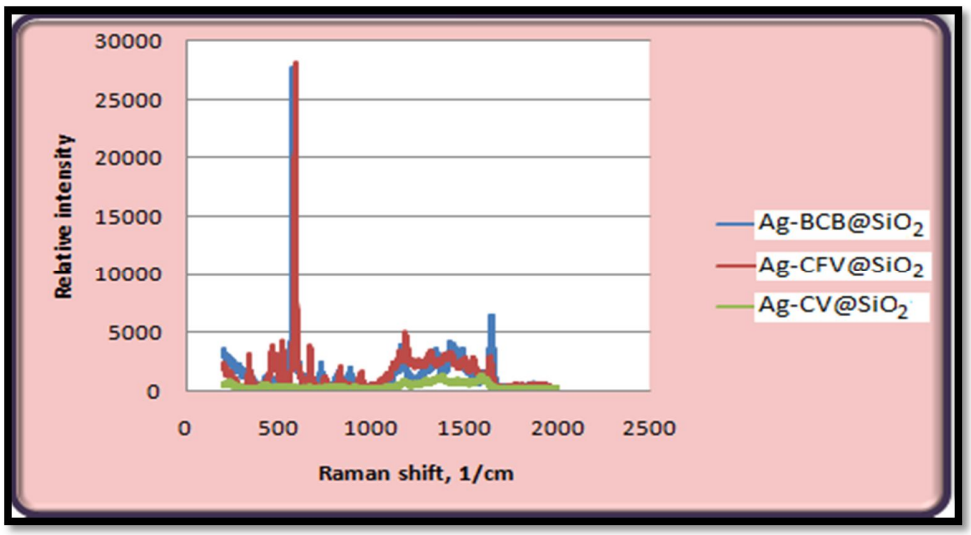

Figure 3.20 Raman spectra of Ag-BCB@SiO_2, Ag-CFV@SiO_2, Ag-CV@SiO_2 SERS nanotags prepared using embedding method for $[dye]_{rxn}$ is 10^{-3} M and [TEOS]/[water] is $9x10^{-4}$.

As seen in the Raman spectra (Figure 3.22) the intensities of Ag-BCB@SiO_2 and Ag-CFV@SiO_2 nanotags are almost the same whereas Ag-CV@SiO_2 nanotag yields very weak signal intensity in comparison with the other two. In order to be able to differentiate the superimposed spectra of Ag-BCB@SiO_2 and Ag-CFV@SiO_2 from each other, their Raman spectra are also presented at a shorter wavenumber region (400 to 800 cm^{-1}) in Figure 3.21.

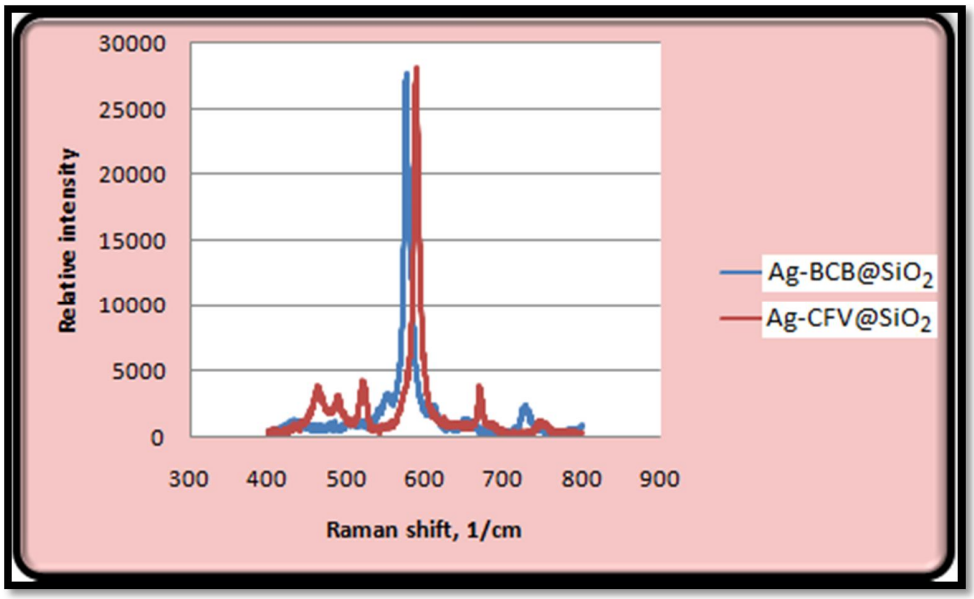

Figure 3.21 Raman spectra of Ag-BCB@SiO_2 and Ag-CFV@SiO_2 SERS nanotags prepared using embedding method for $[dye]_{rxn}$ is 10^{-3} M and [TEOS]/[water] is $9x10^{-4}$.

As can be seen in Figure 3.21, although two characteristic peaks of dyes BCB and CFV stands very closely to each other, they can be resolved clearly due to the narrow peak widths of Raman signals. This spectra carries a crucial importance for this study, showing that both Ag-BCB@SiO_2 and Ag-CFV@SiO_2 exhibit similar and very strong

Raman signals. In other word, BCB and CFV can be used to prepare dual dye doped nanotags having various dye concentration ratios in the same Ag-SiO_2 nanoparticles.

In the preparation of multiple-dye doped SERS nanotags, the same strategy was applied as in the case of preparation of single dye-doped SERS nanotags. In the embedding method, Ag nanoparticles were first treated with solutions of dyes BCB and CFV at ratios BCB:CFV = 1:1, 1:0.8, 1:0.6, and 1:0.4 and then coated with silica using Procedure A. Individual Raman spectrum of these multiple dye-doped nanotags are depicted in Figure 3.22, respectively.

a.

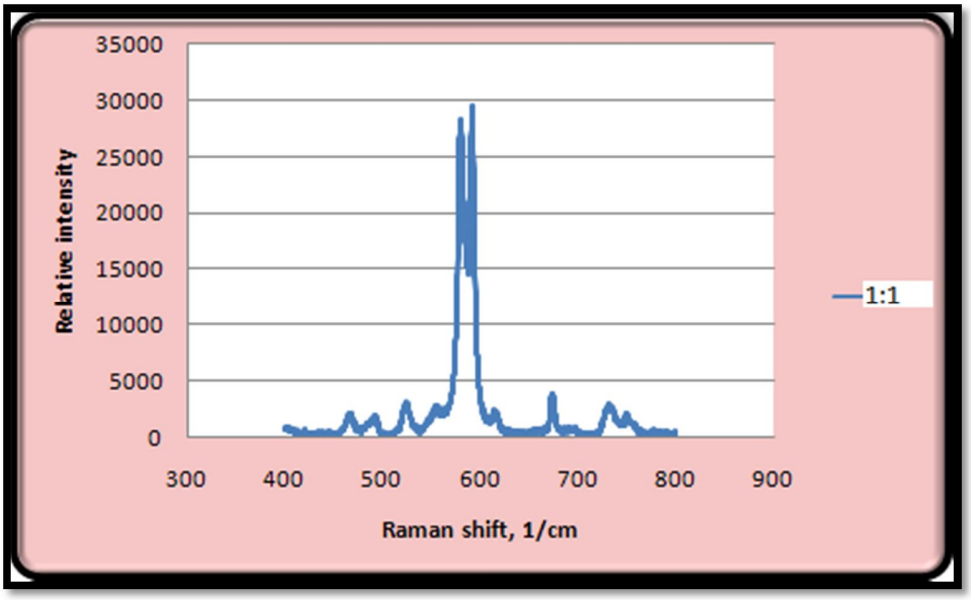

b.

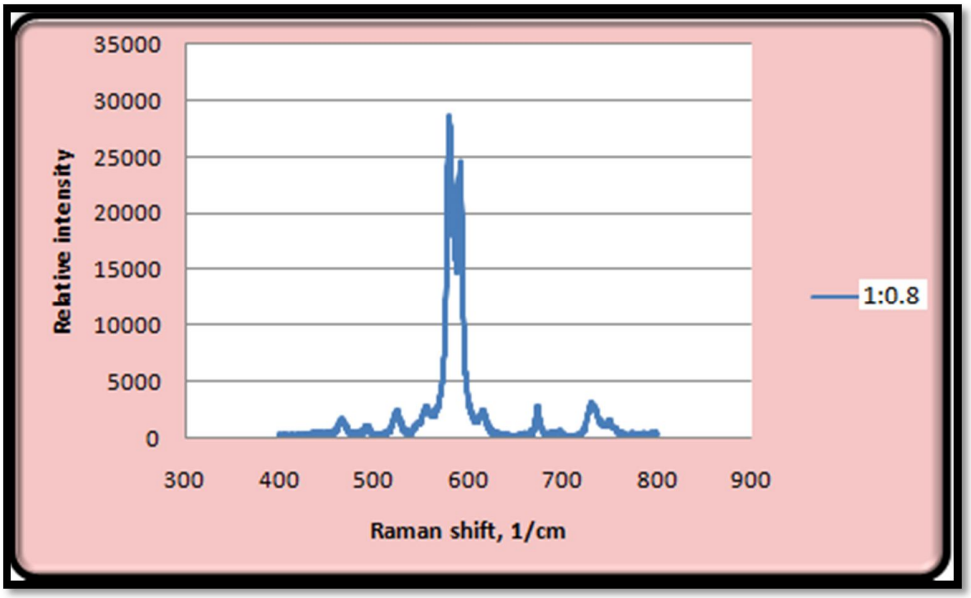
35000
30000
25000
20000
15000
10000
5000
0
Relative intensity
300
400
500
600
700
800
900
Raman shift, 1/cm
1:0.8

c.

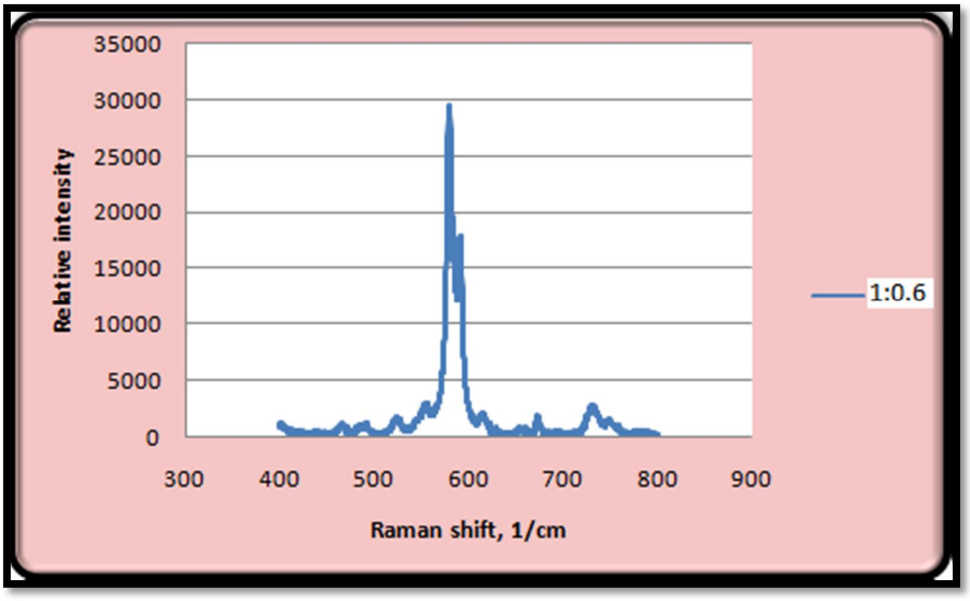
35000
30000
25000
20000
15000
10000
5000
0
Relative intensity
300
400
500
600
700
800
900
Raman shift, 1/cm
1:0.6

d.

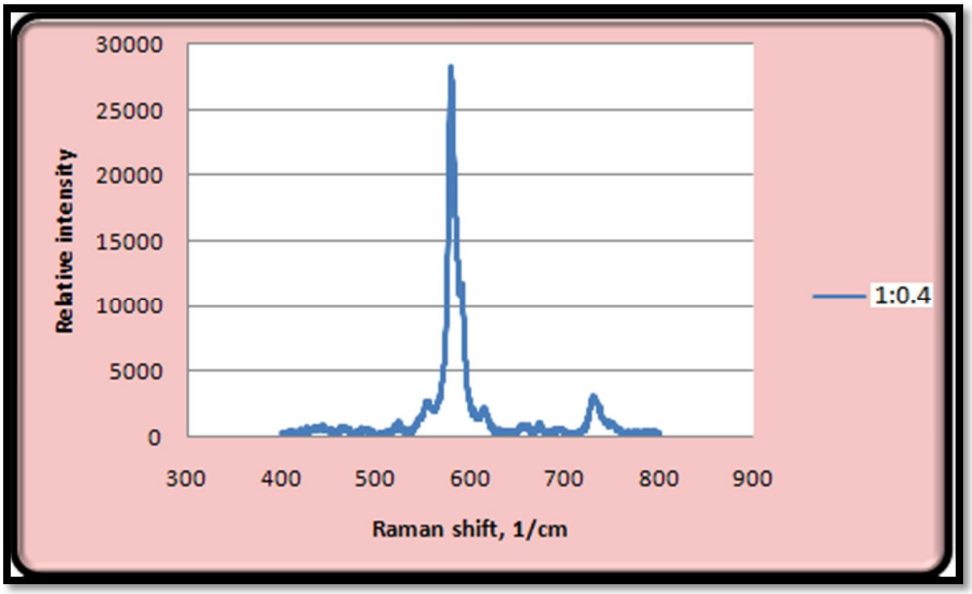

Figure 3.22 Raman spectra of Ag-BCB-CFV@SiO_2 SERS nanotags prepared by varying [BCB]:[CFV] as a. 1:1, b. 1:0.8, c. 1:0.6, and d. 1:0.4 in the embedding method for $[BCB]_{rxn}$ is 10^{-3} M and [TEOS]/[water] is $9x10^{-5}$.

The resultant Raman spectra of Ag-BCB-CFV@SiO_2 nanotags having various mole ratios of two Raman dyes (Figure 3.22) proved successful doping of multiple dyes inside the same nanoparticle and illustrated that direct mixing of multiple dye species at the initial particle surfaces was a useful approach for creating particles for multiplexing studies. As shown in Figure 3.22, the concentration of BCB was kept constant while the concentration of CFV was varied. In order to visualize the increase in the signal of the CFV in those nanotags, their Raman spectra were superimposed and presented in Figure 3.23.

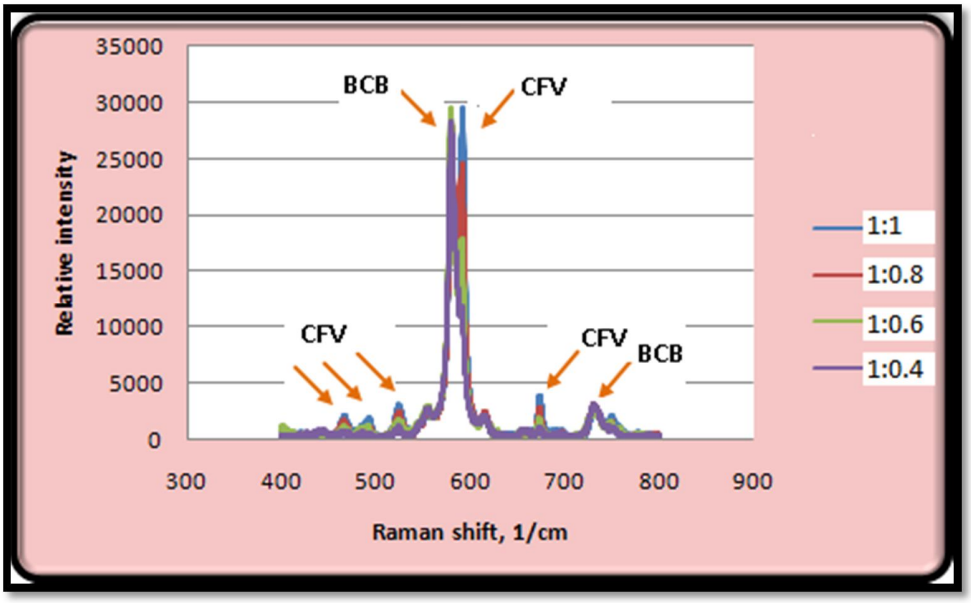

Figure 3.23 Raman spectra of combining spectrum of each Ag-BCB-CFV@SiO_2 SERS nanotags prepared by varying [BCB]:[CFV] as 1:1, 1:0.8, 1:0.6, and 1:0.4 in the embedding method for $[BCB]_{rxn}$ is 10^{-3} M and [TEOS]/[water] is $9x10^{-5}$.

The Raman intensity of the CFV for each of the four SERS tags were easily identified with their corresponding colors (Figure 3.23) and visually their intensities were correlated well with increasing CFV concentration particularly at 591 cm^{-1}. As can also be seen in Figure 3.23, BCB peaks differ from CFV peaks at 580 and 730 cm^{-1} whereas CFV is distinguishable at around 466, 470, 525 and 673 cm^{-1}. These fingerprint spectra make it possible to utilize different intensity ratio at different regions of the spectrum corresponding to the doping ratio. Here, three peaks of CFV (591; 673; 525 cm^{-1}) and two peaks of BCB (580 an 730 cm^{-1}) were taken into consideration. The signal intensities of CFV and BCB at these wave numbers were measured and BCB to CFV ratio was calculated. The extended Raman spectra of nanotags at around 591, 673 and 525

cm^{-1} are given in Figures 3.24, 3.26 and 3.28, respectively. The intensity ratios of BCB to CFV at the corresponding regions (BCB (580 cm^{-1})/CFV (591 cm^{-1}); BCB (580 cm^{-1})/CFV (673 cm^{-1}); BCB (730 cm^{-1})/CFV (525 cm^{-1})) regarding to their molar ratios are summarized in Table 3.5 -3.7. The correlation between the aforementioned signal intensity ratios to the molar ratios are presented in Figures 3.25, 3.27 and 3.29, respectively.

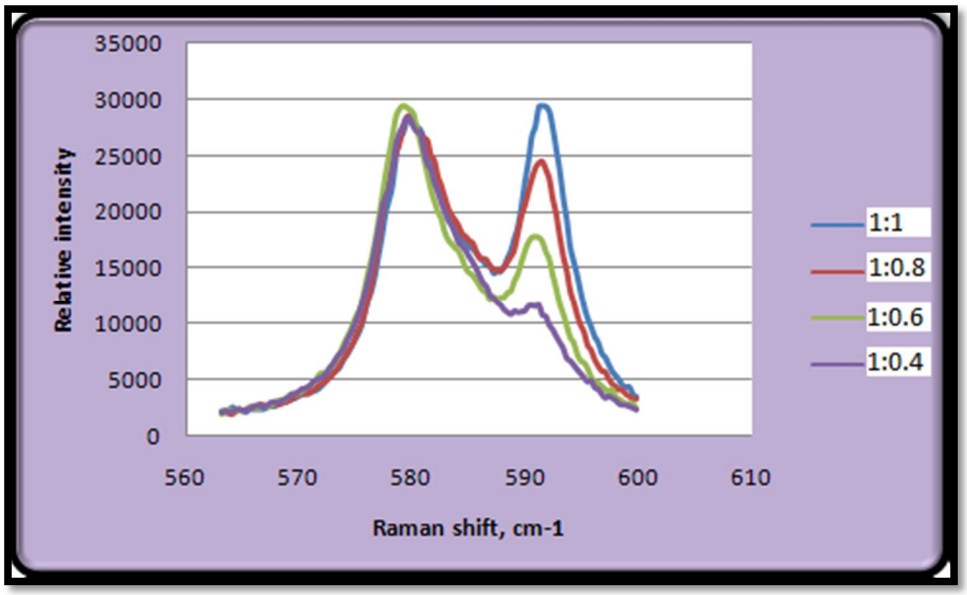

Figure 3.24 Raman spectra of Ag-BCB-CFV@SiO_2 nanotags in which 591 cm^{-1} was taken as reference for CFV intensity against the BCB intensity at 580 cm^{-1}.

Table 3.4 Intensity ratio of BCB (580 cm^{-1}) to CFV (591 cm^{-1}) in Ag-BCB-CFV@ SiO_2 nanotag corresponding to the doping ratio, [BCB]/[CFV].

Doping ratio, [BCB]/[CFV]	**Intensity ratio, I_{BCB} (580 cm^{-1}) / I_{CFV} (591 cm^{-1})**
1:1 (=1.00)	0.96
1:0.8 (=1.25)	1.17
1:0.6 (=1.67)	1.65
1:0.4 (=2.50)	2.4

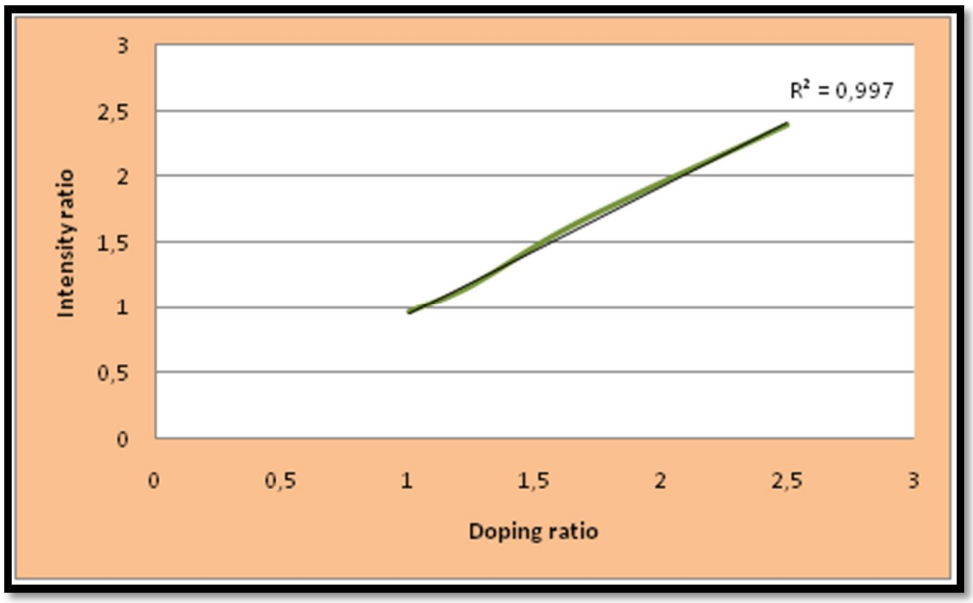

Figure 3.25 Correlation of intensity ratio (I_{BCB}/I_{CFV}) with regard to doping ratio ([BCB]/[CFV]) when the reference peaks locate on 580 and 591 cm^{-1} for BCB and CFV, respectively.

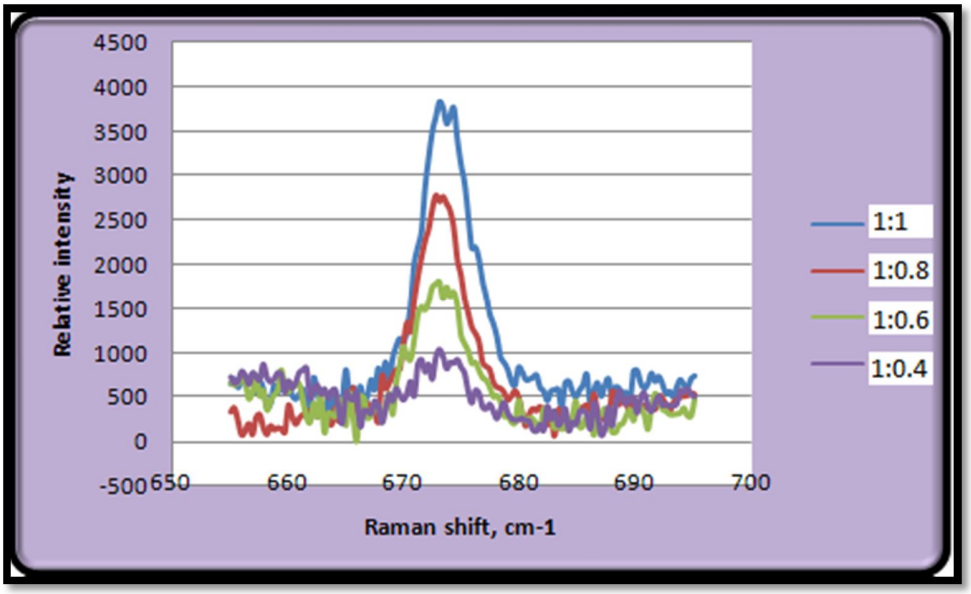

Figure 3.26 Raman spectra of Ag-BCB-CFV@SiO_2 nanotags in which 673 cm^{-1} was taken as reference for CFV intensity against the BCB intensity at 580 cm^{-1}.

Table 3.5 Intensity ratio of BCB (580 cm^{-1}) to CFV (673 cm^{-1}) in Ag-BCB-CFV@ SiO_2 nanotag corresponding to the doping ratio, [BCB]/[CFV].

Doping ratio, [BCB]/[CFV]	**Intensity ratio, I_{BCB} (580 cm^{-1}) / I_{CFV} (673 cm^{-1})**
1:1 (=1.00)	7.35
1:0.8 (=1.25)	10.31
1:0.6 (=1.67)	16.17
1:0.4 (=2.50)	26.98

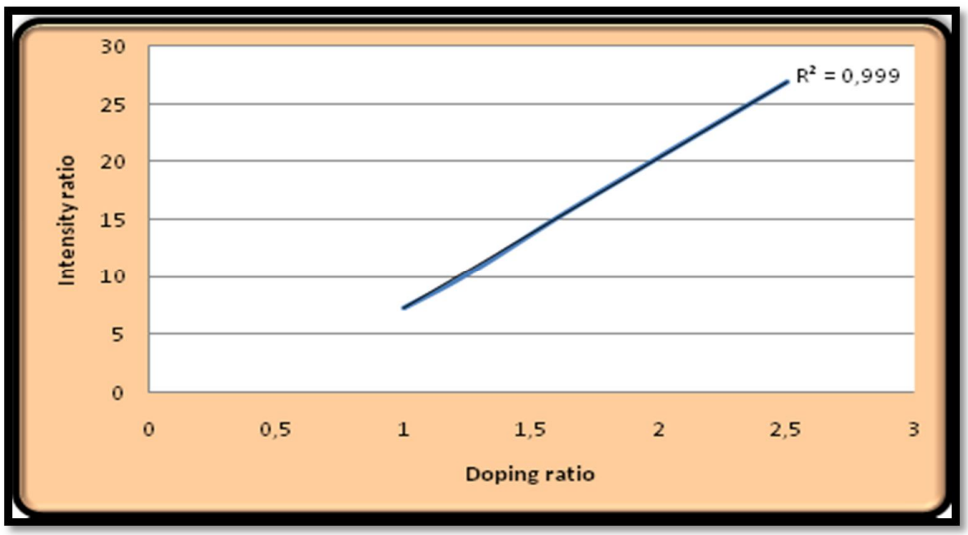

Figure 3.27 Correlation of intensity ratio (I_{BCB}/I_{CFV}) with regard to doping ratio ([BCB]/[CFV]) when the reference peaks locate on 580 and 673 cm^{-1} for BCB and CFV, respectively.

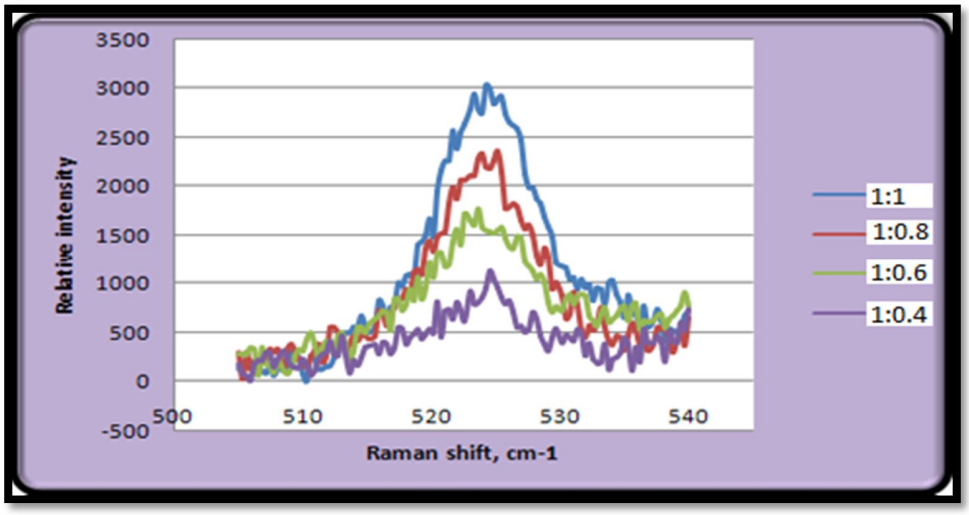

Figure 3.28 Raman spectra of Ag-BCB-CFV@SiO_2 nanotags in which 525 cm^{-1} was taken as reference for CFV intensity against the BCB intensity at 730 cm^{-1}.

Table 3.6 Intensity ratio of BCB (730 cm^{-1}) to CFV (525 cm^{-1}) in Ag-BCB-CFV@ SiO_2 nanotag corresponding to the doping ratio, [BCB]/[CFV].

Doping ratio, **[BCB]/[CFV]**	**Intensity ratio,** **I_{BCB} (730 cm^{-1}) / I_{CFV} (525 cm^{-1})**
1:1 (=1.00)	0.97
1:0.8 (=1.25)	1.32
1:0.6 (=1.67)	1.74
1:0.4 (=2.50)	2.72

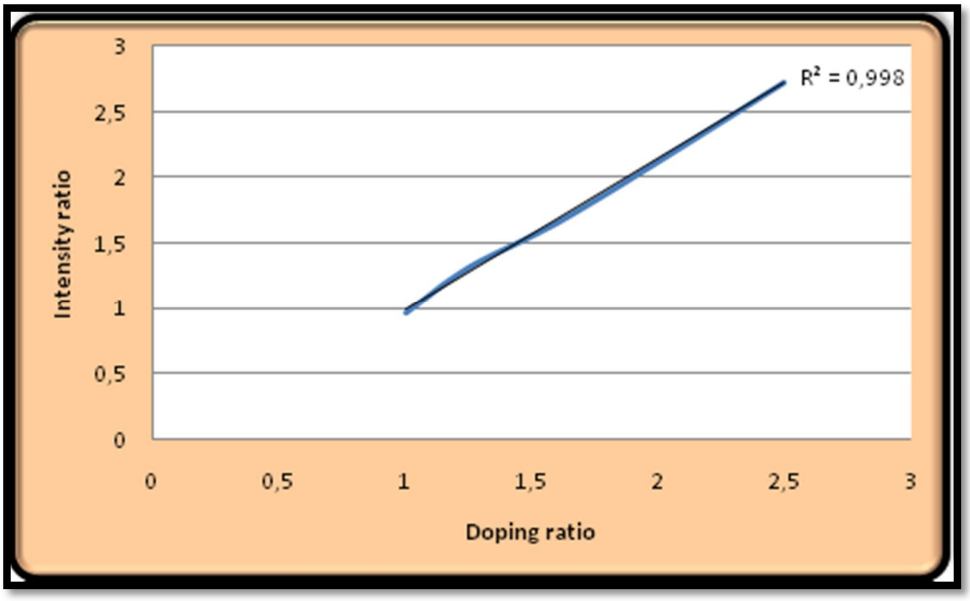

Figure 3.29 Correlation of intensity ratio (I_{BCB}/I_{CFV}) with regard to doping ratio ([BCB]/[CFV]) when the reference peaks locate on 730 and 525 cm^{-1} for BCB and CFV, respectively.

The very high correlation coefficients (0.997; 0.999, 0.998) obtained from the plots of BCB/CFV intensity ratios versus their molar ratios (Figures 3.25, 3.27 and 3.29, respectively) showed that whenever necessary, all these peaks can be used to identify these dyes.

CHAPTER 4

CONCLUSION

When a nanoparticle is used as a Raman probe, a large number of Raman reporter are encapsulated inside this single nanoparticle, which produces a strong Raman signal when it is excited properly. The aim of this thesis was to develop a new nanotag system for the detection of biological molecules by Surface Enhanced Raman Spectroscopy (SERS). In this sense, by use of the facilities of nanotechnology, two groups of SERS nano tags were prepared in order to increase the signal and sensitivity of the SERS analysis.

First group was single-dye doped nanotags, namely Ag-BCB@SiO_2,Ag-CFV@SiO_2 and Ag-CV@SiO_2 and the second group was multi-dye doped nanotags, namely Ag-BCB-CFV@SiO_2. Moreover, by doping two dyes at various ratios in the same Ag-SiO_2 nanoparticle, the variety of SERS Ag-BCB-CFV@SiO_2 nanotag was greatly expanded. In their preparation, positively charged dyes, brilliant cresyl blue (BCB), cresyl fast violet (CFV) and cresyl violet (CV) were used and the electrostatic attraction between the surface and the dyes were explored. All of the prepared SERS nanotags were legible in Raman microscopy and showing a promising ability in multiplexing bioanalysis.

To our knowledge, this is the first time for the encapsulation of BCB and CFV in silver – silica core shell nanoparticles as a SERS nanotag (Ag-BCB@SiO_2 and Ag-CFV@SiO_2) .In addition, this is the first study that reports the doping of two different dyes at various ratios in the same metal nanoparticle covered with a silica shell as a SERS nanotag.

REFERENCE

1. Yih T. C., Talpasanu I. *Micro and Nano Manipulations for Biomedical Applications*, **2008**, Artech House, Norwood.

2. Hornyak G. L., Moore J. J., Tibbals H. F., Dutta J. *Fundamentals of Nanotechnology*, **2009**, CRC Press, New York.

3. Wang L., Wang K., Santra S., Zhao X., Hillard L. R., Smith J. E., Wu Y., Tan W. *Analytical Chemistry*, **2006**, 647-654.

4. Yan J., Estévez M. C., Smith J. E., Wang K. He X., Wang L., Tan W. Yan, *Nanotoday*, **2007**, 3 (2), 44-50.

5. Kumar C., *Nanomaterials for Medical Diagnosis and Therapy*, **2007***,* Wiley-VCH, Weinheim.

6. Zhao X., Tapec-Dytioco R., Tan W., *J. Am. Chem. Soc.*, **2003**, 38 (125), 11474–11475.

7. Feynman R. P., *Engineering and Science*, **1960**, 23 (5), 1-13.

8. Tourney C., *Nature Nanotechnology*, **2009**, 4, 783-784.

9. Scott E. M., *Journal of Leukocyte Biology*, **2005**, 78, 585-594.

10. Wen-Tso L., *Journal of Bioscience and Bioengineering*, **2006** , 102 (1), 1–7.

11. Li X., Du X., He J., *Langmuir*, **2010**, 26 (16), 13528–13534.

12. Wang H., Hu Y., Zhang L., Li C., *Ind. Eng. Chem. Res.*, **2010**, 49 (8), 3654–3662.

13. Kim J. S., Kuk E., Yu K. N., Kim J. H., Park S. J., Lee H. J., Kim S. H., Park Y. K., Park Y.H., Hwang C. Y., Kim Y. K., Lee Y. S., Jeong D. H., Cho M. H., *Nanomedicine: Nanotechnology, Biology and Medicine*, **2007**, 3 (1), 95-101.

14. Ren G., Hu D., Cheng E. W. C., Vargas-Reus M. A., Reip P., Allaker R.P., *International Journal of Antimicrobial Agents*, **2009**, 33 (6), 587-590.

15. Osaka T., Matsunaga T., Nakanishi T., Arakaki A., Niwa D., Iida H., *Anal Bioanal Chem*, **2006**, 384, 593–600.

16. Lu Y., Lu X., Mayers B. T., Herricks T., Xia. Y., *Journal of Solid State Chemistry*, **2008**, 181 (7), 1530-1538.

17. Lili L., Liming M., Xuechen D., *Materials Research Bulletin*, **2006**, 41(9), 541-546.

18. Pany W., Zhang H., Chen. Y., *J. Mater. Sci. Technol.*, **2009**, 25 (2), 247-250.

19. Song J. E., Kim Y. H., Kang Y. S., *Current Applied Physics* , **2006**, 6 (4), 791-795.

20. Kathirvelu S., D'Souza L., Dhurai B., *Indian Journal of Fibre & Textile Research*, **2009**, 34, 267-273.

21. Sato T., Yin S., *Phosphorous Research Bulletin*, **2010**, 24, 43-48.

22. Hu Y. Q., Zhou S. X., Wu L. M., *Polymer*, **2009**, 50 (15), 3609-3616.

23. Li T., Chen Q., Schadler L. S., Siegel R. W., Mendel J., Irvın G. C. Jr., *Polymer Composites*, **2002**, 23 (6), 1076-1086.

24. Hwang D.K., Moon J.H., Shul Y.G., Jung K.T., Kim D.H., Lee D.W., *Journal of Sol-Gel Science and Technology*, **2003**, 26, 783–787.

25. Chen Y., Wang Q., Yan W., Tang H., *Polymer Degradation and Stability*, **2006**, 91 (11), 2632-2643.

26. Hikita M., Nakamura T., Tanaka K., Takahara A., Kajiyama T., *Langmuir*, **2005**, 21, 7299-7302.

27. Soeno T., Inokuchi K., Shiratori S., *Applied Surface Science*, **2004**, 237, 543–547.

28. Jwo C. S., Jeng L. Y., Chang H., Teng T.P., *Rev.Adv.Mater.Sci.*, **2008**, 660-666.

29. Lee K., Hwang Y., Cheong S., Kwom L., Kim S., Lee J., *Current Applied Physics*, **2009**, 9, e128–e131.

30. Güneş S., Fritz K. P., Neudebauera H., Sarıçiftçi N. S., Kumar S., Scholes G. D., *Solar Energy Materials & Solar Cells* ,**2007**, 91, 420–423.

31. Law M., Greene L. E., Johnson J. C., Saykally R., Yang P., *Nature Materials*, **2005,** 2, 455-459.

32. Chowdhuri A., Gupta V., Sreenivas K., Kumar R., Mozumdar S., Patanjali P.K., *Applied Physics Letters*, **2004**, 84 (7), 1180-1182.

33. Lutic D., Strand M., Lloyd-Spetz A., Buchholt K., Ieva E., Käll P. O., Sanati M., *Topics in Catalysis*, **2007**, 45, 105-109.

34. Lu G., Huebner K. L., Ocola L. E., Gajdardziska-Josifovska M., Chen J., *Journal of Nanomaterials*, **2006**, 1-7.

35. Chon J. W. M., Bullen C., Zijlstra P., Gu M., *Adv. Funct. Mater.*, **2007**, 17, 875–880.

36. Ethirajan A., Wiedwald U., Boyen H. G., Kern B., Han L., Klimmer A., Weigl F., Kästle G., Ziemann P., Fauth K., Cai J., Behm R. J., Romanyuk A., Oelhafen P., Walther P., Biskupek J., Kaiser U., A*dv. Mater.*,**2007**, 19, 406–410.

37. Srimani D., Sawoo S., Sarkar A., *Org. Lett.*, **2007**, 9 (18), 3619-3642.

38. Metin Ö., Mazumder V., Özkar S., Sun S., *J. Am. Chem. Soc.,* **2010**, 132, 1468–1469.

39. Arrebola J. C., Caballero A., Hernán L., Morales J., *Journal of Nanomaterials*, **2008**, 1-10.

40. Wu Z. S., Ren W., Wen L., Gao L., Zhao J., Chen Z., Zhou G., Li F., Cheng H. M., *ACS Nano*, **2010**, 4 (6), 3187–3194 .

41. Kokura S., Handa O., Takagi T., Ishikawa T., Naito Y., Yoshikawa T., *Nanomedicine*, **2010**, 6 (4), 570-574.

42. Cengiz E., Wissing S. A., Müller R. H., Yazan Y., *International Journal of Cosmetic Science*, **2006**, 28, 371–378.

43. Ai F., Zheng H., Wei M., Huang J., *Journal of Applied Polymer Science*, **2007**, 105, 1597–1604.

44. Hongxia Y., Pengbo L., Junping Z., Rongchang N., *Journal of Reinforced Plastics and Composites*, **2010**, 29 (10), 1515-1522.

45. Khaydarov R. A., Khaydarov R. R., Gapurova O., *Water Reseach*, **2010**, 44, 1927-1933.

46. Prashant J., Pradeep T., *Biotechnology and Bioengineering*, **2005**, 90 (1), 59-63.

47. Sousa M. H., Hasmonay E., Depeyrot J., Tourinho F.A., Bacri J.C., Dubois E., Perzynski R., Raikher Y.L., *Journal of Magnetism and Magnetic Materials*, **2002**, 572–574.

48. Li J., Dai D., Zhao B., Lin Y., Liu C, *Journal of Nanoparticle Research*, **2002**, 4, 261–264.

49. http://dcstem.pbworks.com/Nanotechnology.

50. Salata O., *Journal of Nanobiotechnology*, **2004** , 2, 1-6.

51. Shimizu K., Ito A., Arinobe M., Murase Y., Iwata Y., Narita Y., Kagami H., Ueda M., Honda H., *Journal of Bioscience and Bioengineering*, **2007**, 103 (5), 472–478.

52. Visaria R. K., Griffin R. J., Williams B. W., Ebbini E. S., Paciotti G. F., Song C. W., Bischof J. C., *Mol Cancer Ther*, **2006**, 5 (4), 1014-1020.

53. Johannsen M., Gneveckow U., Eckelt L., Feussner A., Waldöfner N., Scholz R., Deger S., Wust P., Loening S. A.,; Jordan A., *Int. J. Hyperthermia*, **2005**, 21 (7), 637–647.

54. Babes L., Denizot B., Tanguy, G., Jeune J. J. L., Jallet P., *Journal of Colloid and Interface Science*, **1999**, 212, 474–482.

55. Reynolds C. H., Annan N., Beshah K., Huber J. H., Shaber S. H., Lenkinski R. E., Wortman J A., *J. Am. Chem. Soc.*, **2000**, 122, 8940-8945.

56. Bowman K., Leong K W., *International Journal of Nanomedicine*, **2006**, 1 (2), 117–128.

57. Han G., Ghosh P., De M., Rotello V. M., *Nanobiotechnol*, **2007**, 3, 40-45.

58. Chen W., Shen H., Li X., Jia N., Xu J., *Applied Surface Science*, **2006**, 253, 1762–1769.

59. Lee I. S., Lee N., Park J., Kim B. H., Yi Y. W., Kim T., Kim T. K., Lee I. H., Paik S. R., Hyeon T., *J. Am. Chem. Soc.*, **2006**, 128, 10658-10659.

60. Stoeva S. I., Lee J. S., Smith J. E., Rosen S. T., Mirkin C. A., *J. Am. Chem. Soc.*, **2006**, 128, 8378-8379.

61. Kasili P. M., Wabuyele M. B., Vo-Dinh T., *NanoBiotechnology*, **2006**, 2, 29-35.

62. Sengupta A., Mujacic M., Davis E., *J. Anal Bioanal Chem*, **2006**, 386, 1379–1386.

63. Li X. X., Cao C., Han S. J., Sim S. J., *Water Research*, **2009,** 4 (3), 1425-1431.

64. Taylor J. R., Fang M. M., Nie S., *Anal. Chem.*, **2000**, 72, 979-1986.

65. Liu C. H., Li Z. P., Du B. A., Duan X.R., Wang Y. C., *Anal. Chem.*, **2006**, 78, 3738-3744.

66. Alivisatos A. P., Gu W. W., Larabell C. A., *Annu. Rev. Biomed. Eng.*, **2005**, 7, 55-76.

67. Chan W. C. W., Nie S., *Science*, **1998**, 281, 2016-2018 .

68. Hardman R., *Environmental Health Perspectives*, **2006**, 114 (2), 165-172.

69. Ye Z., Tan M., Wang G., Yuan J., *J. Mater. Chem.*, **2004**, 14, 851-856.

70. Knopp D., Tang D., Niessner R., *Analytica Chimica Acta*, **2009**, 647 (1), 14-30.

71. Sivakumar S., Diamente P. R., Veggel F. C. J. M., *Chem. Eur. J.*, **2006**, 12, 5878 – 5884.

72. Di W., Li J., Shirahata N., Sakka Y., *Nanotechnology*, **2010**, 21, 1-8.

73. Estévez M. C., O'Donoghue M. B., Chen X., Tan W., *Nano Res*, **2009**, 2, 448-461.

74. Santra S., Wang K. M., Tapec R. U., Tan W. H., *Journal of Biomedical Optics*, **2001**, 6 (2), 160–166.

75. Zhao X., Bagwe R. P., Tan W. H., *Adv. Mater.*, **2004**, 16 (2), 173-176.

76. Aslan K., Holley P., Geddes C. D., *J. Mater. Chem.*, **2006**, 16, 2846–2852.

77. Geddes C. D., Lakowicz J. R., *Journal of Fluorescence*, **2002**, 12 (2), 121-129.

78. Aslan K., Wu M., Lakowicz J. R., Geddes C. D., *J. Am. Chem. Soc.*, **2007**, 129, 1524-1525.

79. Vo-Dinh T., Yan F., Wabuyele M. B., *Surface-Enhanced Raman Scattering – Physics and Applications, Topics Appl. Phys.*, **2006**, 103, 409–426.

80. Raman C. V., *Molecular Diffraction of Light,* **1922**, Calcutta University Press, Calcutta.

81. http://www.thefullwiki.org/Chandrasekhara_Venkata_Raman.

82. Smith E., Dent G., *Modern Raman spectroscopy A Practical Approach*, **2005**, John Wiley&Sons Ltd., West Sussex.

83. Mahadevan-Jansen A., Richards-Kortum R., *19th International Conference*, **1997**, Chicago, 2722-2728.

84. Pelletier M. J., *Analytical Applications of Raman Spectroscopy*, **1999**, Blackwell Science, Oxford.

85. Movasaghi Z., Rehman S., Rehman I. U., *Spectroscopy Reviews*, **2007,** 42, 493–541.

86. Doering W. E., Piotti M.E., Natan M. J., Freeman R. G., *Adv. Mater.*, **2007**, 19, 3100–3108.

87. Fleischmann M.,, Hendra P. J., McQuillan A. J., *Chem. Phys. Lett.*, **1974**, 26, 163.

88. Albrecht M. G., Creighton J. A., *Journal of the American Chemical Society*, **1977**, 99 (15), 5215-5217.

89. Kneipp K., Kneipp H., Itzkan I., Dasari R. R., Feld M. S., *Chem. Rev.*, **1999**, 99, 2957-2975.

90. Moskovits M., R*eviews of Modern Physics*, **1985**, 57 (3), 783-828.

91. Vo-Dinh T., Hiromoto M. Y. K., Begun G. M., Moody R. L., *Anal. Chem.*, **1984**, 56, 1667-1670.

92. Kneipp K., Kneipp H., Itzkan I., Dasari R. R., Feld M. S., *J. Phys.: Condens. Matter*, **2002**, 14, R597–R624.

93. Schatz G. C., Young M. A., Duyne R. P. V., *Surface-Enhanced Raman Scattering – Physics and Applications, Topics Appl. Phys.*, **2006**, 103, 19-46.

94. Doering W. E., Nie S., *J. Phys. Chem. B*, **2002**, 106, 311-317.

95. Kelly K. L., Coronado E., Zhao L. L., Schatz G. C. J., *Phys. Chem. B*, **2003**, 107, 668-677.

96. Campion A., Kambhampati P., *Chemical Society Reviews*, **1998**, 27, 241-250.

97. Ansari D. O., *Raman-Encoded Nanoparticles for Biomolecular Detection and Cancer Diagnostics*, **2008**, Bioengineering, Georgia İnstitute of Technology.

98. Yuen C., Zheng W., Huang Z., *Journal of Innovative Optical Health Sciences*, **2008**, 1 (2), 267-284.

99. Gong J. L., Jiang J. H., Yang H. F., Shen G. L., Yu R. Q., Ozaki Y., *Analytica Chimica Acta*, **2006**, 564, 151–157.

100. Kim J. H., Kim J. S., Choi H., Lee S. M., Jun B. H., Yu K. N., Kuk E., Kim Y. K., Jeong D. H., Cho M. H., Lee Y. S., *Anal. Chem.*, **2006**, 78 (19), 6967-6973.

101. Shen A., Chen L., Xie W., Hu J., Zeng A., Richards R., Hu J., *Adv. Funct. Mater.*, **2010**, 20 (6), 969-975.

102. Lutz B., Dentinger C., Sun L., Nguyen L., Zhang J., Chmura A., Allen A., Chan S., Knudsen B., *Journal of Histochemistry & Cytochemistry*, **2008**, 56(4), 371–379.

103. Faulds K., Barbagallo R. P., Keer J. T., Smith W. E., Graham D., *Analyst*, **2004**, 129, 567-568.

104. Strelau K. K., Kretschmer R., Möller R., Fritzsche W., Popp J., *Anal Bioanal Chem*, **2010**, 396, 1381–1384.

105. Cao Y. C., Jin R., Mirkin C. A., *Science*, **2002**, 297, 1536-1540.

106. Liu X., Knauer M., Ivleva N. P., Niessner R., Haisch C., A*nal. Chem.*, **2010**, 82, 441–446.

107. Doering W. E., Nie S., *Anal. Chem.* , **2003**, 75, 6171-6176.

108. Ethiraj A. S., Hebalkar N., Kharrazi S., Urban J., Sainkar S. R., Kulkarni S.K., *Journal of Luminescence* , **2005**, 114, 15–23.

109. Li J. F., Huang Y. F., Ding Y., Yang Z. L., Li S. B., Zhou X. S., Fan F. R.,; Zhang W., Zhou Z. Y., Wu D. Y., Ren B., Wang Z. L., Tian Z. Q., *Nature*, **2010**, 464, 392-395.

110. Fleger Y., Rosenbluh M., *Research Letters in Optics*, **2009**, 1-5 .

111. Si M.Z., Kang Y.P., Zhang Z.G., *Applied Surface Science*, **2009**, 255, 6007–6010.

112. Šileikaitė A., Prosyčevas I., Puišo J., Juraitis A., Guobiene A., *Materials Science*, **2006**, 12 (4), 287-291.

113. Sergeev B. M., Lopatina L. I., Prusov A. N., Sergeev G. B., *Colloid Journal*, **2005**, 67 (1), 72–78.

114. Leopold N., Lendl B., *J. Phys. Chem. B*, **2003**, 107, 5723-5727.

115. Ershov B. G., Abkhalimov E. V., *Colloid Journal*, **2007**, 69 (5), 579–584.

116. Chau J. L. H., Hsu M. K., Hsieh C. C., Kao C. C., *Materials Letters*, **2005**, 59, 905–908.

117. Meziani M. J., Pathak P., Beacham F., Allard L.F., Sun Y. P., *J. of Supercritical Fluids,* **2005**, 34, 91–97.

118. Ji M., Chen X., Wai C. M, Fulton J. L., J*. Am. Chem. Soc.*, **1999**, 121, 2631-2632.

119. Li Z., Li Y., Qian X. F., Yin J., Zhu Z. K., *Applied Surface Science*, **2005**, 250, 109–116.

120. Pfleger J., Šmejkal P., Vlčková B., Miroslav Š., *Advanced Organic and Inorganic Optical Materials*, **2003**, 5122, 198-205.

121. Tang Z., Liu S., Dong S., Wang E., *Journal of Electroanalytical Chemistry*, **2001**, 502, 146–151.

122. Zhu J., Liu S., Palchik O., Koltypin Y., Gedanken A., *Langmuir*, **2000**, 16, 6396-6399.

123. Wang L., Tan. W., Nano Lett., 2006, 6 (1), 84–88.

124. Ung T., Liz-Marzán L. M., Mulvaney P., *Langmuir*, **1998**, 14 (14), 3740–3748.

125. Bagwe R. P., Yang C., Hilliard L. R., Tan W., *Langmuir* , **2004**, 20 (19), 8336–8342.

126. Stöber W., Fink A., *Journal of Colloid and Interface Science*, **1968**, 26, 62-69 .

127. Lutz B. R., Dentinger C. E., Nguyen L. N., Sun L., Zhang J., Allen A. N., Chan S., Knudsen B. S., *ACS Nano.*, **2008**, 2 (11), 2306–2314.

128. Zavaleta C. L., Smith B. R., Walton I., Doering W., Davis G., Shojaei B., Natan M. J., Gambhir S. S., *PNAS*, **2009**, 106 (32), 13511–13516.

129. Chen X., Estévez M. C., Zhu Z., Huang Y. F., Chen Y., Wang L., Tan W., *Anal. Chem.*, **2009**, 81, 7009-7014.

130. Wang L., Yang C., Tan W., *Nano Letters*, **2005**, 5 (1), 37-43.

131. Gellner M., Kömpe K., Schlücker S., *Anal Bioanal Chem*, **2009**, 394, 1839–1844.

132. Wang H. N., Vo-Dinh T., *Nanotechnology*, **2009**, 20, 065101.

133. Kang T., Yoo S. M., Yoon I., Lee S. Y., Kim B., *Nano Lett.*, **2010**, 10, 1189–1193.

134. Lowe A. J., Huh Y. S., Strickland A. D., Erickson D., Batt C. A., *Anal. Chem.*, **2010**, 82, 5810-5814.

135. Kennedy D. C., Hoop K. A., Tay L. L., Pezacki J. P., *Nanoscale*, **2010**, 2, 1413–1416.

136. Sun L., Yu C., Irudayaraj J., *J. Anal Chem.*, **2007**, 79 (11), 3981–3988.

137. Braun G. B., Lee S. J., Laurence T., Fera N., Fabris L., Bazan G. C., Moskovits M., Reich N. O., *Journal of Physical Chemistry C* , **2008**, 1-23.

138. Yu K. N., Lee S. M., Han J. Y., Park H., Woo M. A., Noh M. S., Hwang S. K., Kwon J. T., Jin H., Kim Y. K., Hergenrother P. J., Jeong D. H., Lee Y. S., Cho M. H., *Bioconjugate Chem.*, **2007**, 18, 1155-1162.

139. Lee S., Joo S., Park S., Kim S., Kim H. C., Chung T. D., *Electrophoresis*, **2010**, 31, 1–7.

140. Lee P. C., Meisel D., *J. Phys. Chem.*, **1982**, 86, 3391-3395.

141. Tan S., Erol M., Attygalle A., Du H., Sukhishvili S. L, *Langmuir*, **2007**, 23, 9836-9843.

142. Huang Y., Yang Y., Chen Z., Li X., Nogami M., *J Mater Sci*, **2008**, 43, 5390–5393.

143. Rodríguez-González B., Sánchez-Iglesias A., Giersig M., Liz-Marzán L. M., *Faraday Discuss.*, **2004**, 125, 133–144.

144. Volkan M., Stokes D. L., Vo-Dinh T., *Journal of Raman Spectroscopy*, **1999**, 30, 1057-1065.

145. He L., Kim N. J., Li H., Hu Z., Lin M., *J. Agric. Food Chem.*, **2008**, 56 (21), 9843–9847.

146. Brady C. I., Mack N. H., Brown L. O., Doorn S.K., *Anal. Chem.*, **2009** , 81, 7181-7188.